

Brane Tilings and Specular Duality

Amihay Hanany and Rak-Kyeong Seong

*Theoretical Physics Group, The Blackett Laboratory, Imperial College London,
Prince Consort Road, London SW7 2AZ, UK*

E-mail: a.hanany@imperial.ac.uk, rak-kyeong.seong@imperial.ac.uk

ABSTRACT: We study a new duality which pairs $4d \mathcal{N} = 1$ supersymmetric quiver gauge theories. They are represented by brane tilings and are worldvolume theories of D3 branes at Calabi-Yau 3-fold singularities. The new duality identifies theories which have the same combined mesonic and baryonic moduli space, otherwise called the master space. We obtain the associated Hilbert series which encodes both the generators and defining relations of the moduli space. We illustrate our findings with a set of brane tilings that have reflexive toric diagrams.

Contents

1	Introduction	1
2	Brane Tilings and their Moduli Spaces	4
2.1	Brane Tilings, F- and D-term charges, and the Toric Diagram	4
2.2	The Master Space \mathcal{F}^\flat and the Mesonic Moduli Space \mathcal{M}^{mes}	6
3	An introduction to Specular Duality	8
3.1	Toric Duality and Specular Duality	9
3.2	Specular Duality and ‘Fixing’ Shivers	15
4	Model 13 ($Y^{2,2}, \mathbb{F}_2, \mathbb{C}^3/\mathbb{Z}_4$) and Model 15b ($Y^{2,0}, \mathbb{F}_0, \mathbb{C}/\mathbb{Z}_2$)	20
4.1	Brane Tilings and Superpotentials	20
4.2	Perfect Matchings and the Hilbert Series	23
4.3	Global Symmetries and the Hilbert Series	26
4.4	Generators, the Master Space Cone and the Hilbert Series	29
5	Beyond the torus and Conclusions	32
A	Comments on mesonic and baryonic symmetry charges	35
B	Hilbert series of $\text{Irr } \mathcal{F}^\flat$ for Models 13 and 15b	37

1 Introduction

Dualities have vastly contributed towards a better understanding of string theory and beyond. A particular example is mirror symmetry [1–9] which identifies two Type II superstring theories compactified on Calabi-Yau 3-folds whose Hodge numbers are swapped. A similar example, although only true at low energies, is *toric (Seiberg) duality* [10–16]. It relates supersymmetric worldvolume theories of D3-branes on singular toric Calabi-Yau 3-folds which have isomorphic mesonic moduli spaces.

These $4d \mathcal{N} = 1$ supersymmetric field theories have mesonic moduli spaces which are toric Calabi-Yau 3-folds. Their geometry is encoded in a convex lattice polygon called the toric diagram. Furthermore, the theories are best expressed by periodic bipartite graphs on \mathbb{T}^2 , otherwise known as brane tilings [18–24]. They represent the

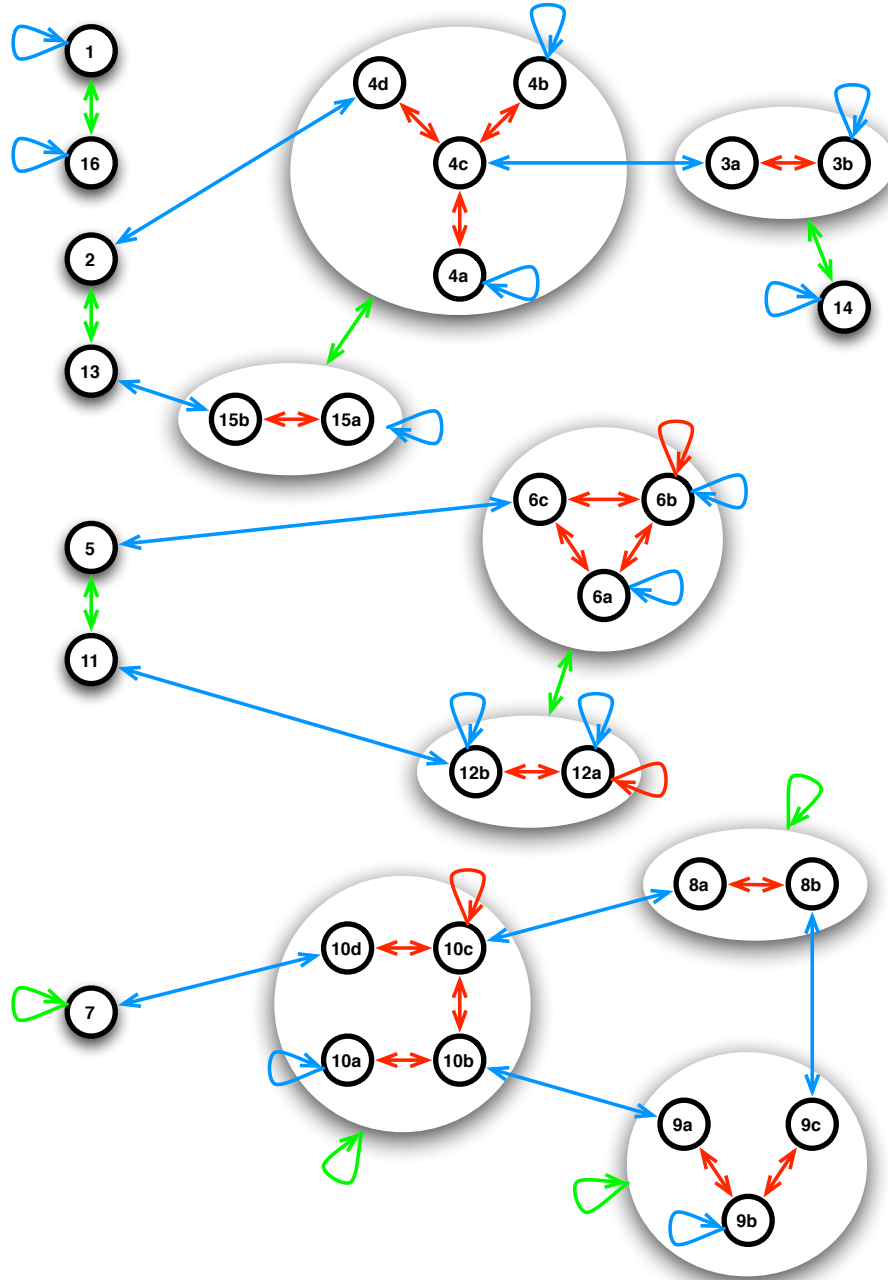


Figure 1. *The three dualities for Brane Tilings with Reflexive Toric Diagrams.* The arrows indicate toric duality (red), specular duality (blue), and reflexive duality (green) which is discussed in [17]. The black nodes of the duality tree represent distinct brane tilings, where the labels are taken from [17] and Figure 3.

largest known class of supersymmetric field theories that are associated to toric Calabi-Yau 3-folds.

The rich combinatorial structure of brane tilings led recently to new insights beyond toric duality. For instance, certain toric diagrams have a single interior point and exhibit the special property of appearing in polar dual pairs [25–30]. They are called reflexive toric diagrams and relate to a correspondence between brane tilings which was studied in [17]. Given brane tilings A and B whose reflexive toric diagrams are a dual pair, the toric diagram of brane tiling A is the lattice of generators of the mesonic moduli space of brane tiling B, and vice versa. We call this correspondence *reflexive duality*.

In the following, we discuss a new correspondence that was named in [17] **specular duality**. It identifies brane tilings which have isomorphic combined mesonic and baryonic moduli spaces, also known as master spaces \mathcal{F}^b . The following scenarios of brane tilings apply to this new duality:

1. Dual brane tilings A and B are both on \mathbb{T}^2 . They have reflexive toric diagrams.
2. Brane tiling A is on \mathbb{T}^2 and dual brane tiling B is not on \mathbb{T}^2 . Brane tiling A has a toric diagram which is not reflexive.
3. Both brane tilings A and B are not on \mathbb{T}^2 .

For brane tilings with reflexive toric diagrams, specular duality manifests itself not only as an isomorphism between master spaces. The additional properties are:

- The external/internal perfect matchings of brane tiling A are the internal/external perfect matchings of brane tiling B.
- The mesonic flavour symmetries of brane tiling A are the hidden or anomalous baryonic symmetries of brane tiling B, and vice versa.

The following paper studies specular duality restricted to brane tilings with reflexive toric diagrams. The Hilbert series of \mathcal{F}^b is computed explicitly to illustrate its invariance under the new correspondence. The swap between external and internal perfect matchings, and mesonic and baryonic symmetries is explained. Moreover, we illustrate that specular duality is a reflection of the Calabi-Yau cone of \mathcal{F}^b along a hyperplane.

The new correspondence extends beyond brane tilings with reflexive toric diagrams. Accordingly, specular duality can lead to brane tilings on spheres or Riemann surfaces with genus $g \geq 2$. These have no known AdS dual and have mesonic moduli spaces

which are not necessarily Calabi-Yau 3-folds [23, 31, 32]. Their quiver and superpotential however admit a master space which can be traced back to a brane tiling on \mathbb{T}^2 .

Specular duality for brane tilings that are not on \mathbb{T}^2 may lead to new insights into quiver gauge theories and Calabi-Yau moduli spaces. The work concludes with this observation and highlights the importance of future studies [33].

The paper is divided into the following sections. Section §2 reviews brane tilings and their mesonic moduli spaces and master spaces. They are analysed with the help of Hilbert series. Section §3 begins with a short review on toric duality and compares its properties with the characteristics of specular duality. The new correspondence between brane tilings is explained in terms of the untwisting map [34–36] and modified shivers [37–39]. Section §4 studies and summarises the transformation of the brane tiling, the exchange of perfect matchings, and the swap of mesonic and baryonic symmetries under specular duality. The concluding section gives a short introduction on how specular duality relates brane tilings on \mathbb{T}^2 with tilings on spheres and Riemann surfaces of genus $g \geq 2$.

2 Brane Tilings and their Moduli Spaces

The following section reviews brane tilings and their mesonic moduli spaces and master spaces. The method of calculating Hilbert series is reviewed. Readers who are familiar with these topics may skip the section and move on to the discussion of specular duality in Section §3.

2.1 Brane Tilings, F- and D-term charges, and the Toric Diagram

A brane tiling represents a worldvolume theory of D3 branes on a singular non-compact Calabi-Yau 3-fold. It encodes the bifundamental matter content and superpotential of the theory.

A **quiver** is a graph which encodes as a set of G nodes the $U(N)_i$ gauge groups and as a set of e arrows the bifundamental fields X_{ij} of the gauge theory. The number of incoming and outgoing arrows is the same at each node. The incidence matrix $d_{G \times e}$ of the graph encodes this property with its vanishing sum of rows.¹ This property is called the quiver’s Calabi-Yau condition [12, 40, 41].

¹ $d_{G \times e}$ can therefore be reduced to its $G - 1$ independent rows $\Delta_{(G-1) \times e}$.

A **brane tiling** or dimer [18–20, 23, 42] is a periodic bipartite graph on \mathbb{T}^2 . It has the following components:

- **Faces** relate to $U(N)_i$ gauge groups. The ranks N of all gauge groups are the same and equal to the number of probe D3-branes.
- **Edges** relate to the bifundamental fields. Every edge X_{ij} in the tiling has two neighbouring faces $U(N)_i$ and $U(N)_j$. The orientation of the bifundamental field X_{ij} is given by the orientation around the black and white nodes at the two ends of the corresponding edge.
- **White (resp. black) nodes** correspond to positive (negative) terms in the superpotential W . They have a clockwise (anti-clockwise) orientation. By following the orientation around a node, one can identify the fields of the related superpotential term in the correct cyclic order.

The geometry of the toric Calabi-Yau 3-fold is encoded in the brane tiling. A new basis of fields is defined from the set of quiver fields in order to describe both F-term and D-term constraints. The new fields are known as gauge linear sigma model (GLSM) fields [43] and are represented as perfect matchings [18, 21, 23, 40] of the brane tiling:

- A **perfect matching** p_α is a set of bifundamental fields which connects to all nodes in the brane tiling precisely once. It corresponds to a point in the toric diagram of the Calabi-Yau 3-fold. A perfect matchings which relates to an **extremal (corner)** point of the toric diagram has non-zero IR $U(1)_R$ charge. An **internal** as well as a non-extremal toric point on the perimeter of the toric diagram has zero R-charge. We call all points on the perimeter **external**, including extremal ones. The number of internal, external and extremal perfect matchings is denoted by n_i , n_e and n_p respectively. All perfect matchings are summarized in a matrix $P_{e \times c}$ [40], where e is the number of matter fields and c the number of perfect matchings. The perfect matching matrix $P_{e \times c}$ takes the form

$$P_{i\alpha} = \begin{cases} 1 & \text{if } X_i \in p_\alpha \\ 0 & \text{if } X_i \notin p_\alpha \end{cases}, \quad (2.1)$$

where $i = 1, \dots, e$ and $\alpha = 1, \dots, c$.

- **F-terms** $\partial_X W = 0$ are encoded in $P_{e \times c}$. The charges under the F-term constraints are given by the kernel,

$$Q_F_{(c-G-2) \times c} = \ker(P_{e \times c}), \quad (2.2)$$

where G is the number of gauge groups.²

- **D-terms** are encoded in the quiver incidence matrix $d_{G \times e}$. The charges Q_D $(G-1) \times c$ under the D-term constraints are defined by

$$\Delta_{(G-1) \times E} = Q_D \ (G-1) \times c \cdot P_{c \times e}^t \ . \quad (2.3)$$

The F- and D-term charge matrices are concatenated to form a total charge matrix

$$Q_t \ (c-3) \times c = \begin{pmatrix} Q_F \\ Q_D \end{pmatrix} \ . \quad (2.4)$$

The kernel of Q_t ,

$$G_t = \ker(Q_t) \ , \quad (2.5)$$

corresponds to a matrix whose columns relate to perfect matchings. The rows of G_t are the coordinates of the associated point in the toric diagram.

2.2 The Master Space \mathcal{F}^b and the Mesonic Moduli Space \mathcal{M}^{mes}

Master Space \mathcal{F}^b . The master space is the combined mesonic and baryonic moduli space. It has the following properties:

- The **master space** [40, 41, 44] of the one D3-brane theory relates to the following quotient ring

$$\mathbb{C}^e[X_1, \dots, X_e] / \mathcal{I}_{\partial W=0} \ , \quad (2.6)$$

where e is the number of bifundamental fields X_i . $\mathbb{C}^e[X_1, \dots, X_e]$ is the complex ring over all bifundamental fields, and $\mathcal{I}_{\partial W=0}$ is the ideal formed by the F-terms.

- The master space in (2.6) is usually reducible into components. The largest irreducible component is known as the **coherent component** ${}^{\text{Irr}}\mathcal{F}^b$ and is toric Calabi-Yau. All other smaller components are generally linear pieces of the form \mathbb{C}^l . In our discussion, we will concentrate on the coherent component of the master space and for simplicity use \mathcal{F}^b and ${}^{\text{Irr}}\mathcal{F}^b$ interchangeably.

²Note: \ker used here takes the transpose of the matrix.

- The coherent component of the master space is the following **symplectic quotient**

$$\text{Irr } \mathcal{F}^{\flat} = \mathbb{C}^c[p_1, \dots, p_c] // Q_F \quad , \quad (2.7)$$

where c is the number of perfect matchings p_α in the brane tiling. The symplectic quotient captures invariants of the ring $\mathbb{C}^c[p_1, \dots, p_c]$ under the charges Q_F in (2.2).

- The **dimension** of the master space \mathcal{F}^{\flat} is $G + 2$.

The master space exhibits the following symmetries:

- The **mesonic symmetry** is $U(1)^3$ or an enhancement with rank 3. An enhancement is indicated by extremal perfect matchings which carry the same Q_F charges. The mesonic symmetry contains the $U(1)_R$ symmetry and the flavor symmetries. It derives from the isometry of the toric Calabi-Yau 3-fold.
- The **baryonic symmetry** is $U(1)^{G-1}$ or an enhancement with rank $G - 1$. An enhancement is indicated by non-extremal perfect matchings which carry the same Q_F charges. It contains both anomalous and non-anomalous symmetries which have decoupling gauge dynamics in the IR. Non-Abelian extensions of these symmetries are known as **hidden symmetries** [40, 41, 44].

Let I and E denote respectively the number of internal and external points in the toric diagram.³ They are used to define the following quantities:

- The number of **anomalous** $U(1)$ baryonic symmetries or the total rank of enhanced **hidden** baryonic symmetries is given by $2I$.
- The number of **non-anomalous** baryonic $U(1)$'s is $E - 3$.
- The total number of baryonic symmetries is as stated above $G - 1$. Accordingly,

$$G - 1 = 2I + E - 3 \Rightarrow A = \frac{G}{2} = I + \frac{E}{2} - 1 \quad (2.8)$$

which is **Pick's theorem** generalised to toric diagrams. The unit square area A of a toric diagram is scaled by a factor of 2 in order to relate it to the number of $U(N)$ gauge groups G .

³Note: Points in the toric diagram can carry multiplicities according to the number of perfect matchings associated to them. I and E is a counting that ignores multiplicities and hence there is no direct correspondence to the number of perfect matchings n_i , n_e and n_p .

Perfect matchings carry charges under the mesonic and baryonic symmetries. The choices of assigning charges on perfect matchings are under certain basic constraints which are summarized in appendix §A.

Mesonic Moduli Space \mathcal{M}^{mes} . The mesonic moduli space is a subspace of the master space. It has the following properties:

- The **mesonic moduli space** for the one D3 brane theory is the following symplectic quotient

$$\mathcal{M}^{mes} = (\mathbb{C}^c[p_1, \dots, p_c] // Q_F) // Q_D = \mathcal{F}^b // Q_D \quad . \quad (2.9)$$

- The mesonic moduli space is a toric Calabi-Yau 3-fold and is generally lower dimensional than the master space.

Hilbert Series. The Hilbert series is a generating function which counts chiral gauge invariant operators. It contains information on moduli space generators and their relations. A method known as **plethystics** [45–47] is used to extract the information from the Hilbert series. For charges Q which are either Q_F or Q_t for $\text{Irr } \mathcal{F}^b$ and \mathcal{M}^{mes} respectively, the corresponding Hilbert series is given by the **Molien Integral**

$$g_1(y_\alpha; \mathcal{M}) = \prod_{i=1}^{|Q|} \oint_{|z_i|=1} \frac{dz_i}{2\pi i z_i} \prod_{\alpha=1}^c \frac{1}{1 - y_\alpha \prod_{j=1}^{|Q|} z_j^{Q_{j\alpha}}} \quad (2.10)$$

where c is the number of perfect matchings and $|Q|$ is the number of rows in the charge matrix Q . The fugacity $y_\alpha = t_\alpha$ counts extremal perfect matchings and the fugacity y_{s_m} counts all other fugacities s_m .

3 An introduction to Specular Duality

The following section reviews toric duality of brane tilings and compares it with specular duality. The section illustrates how the new correspondence is related to the untwisting map [34–36] and the shiver [37–39]. We focus on the 30 brane tilings with reflexive toric diagrams.

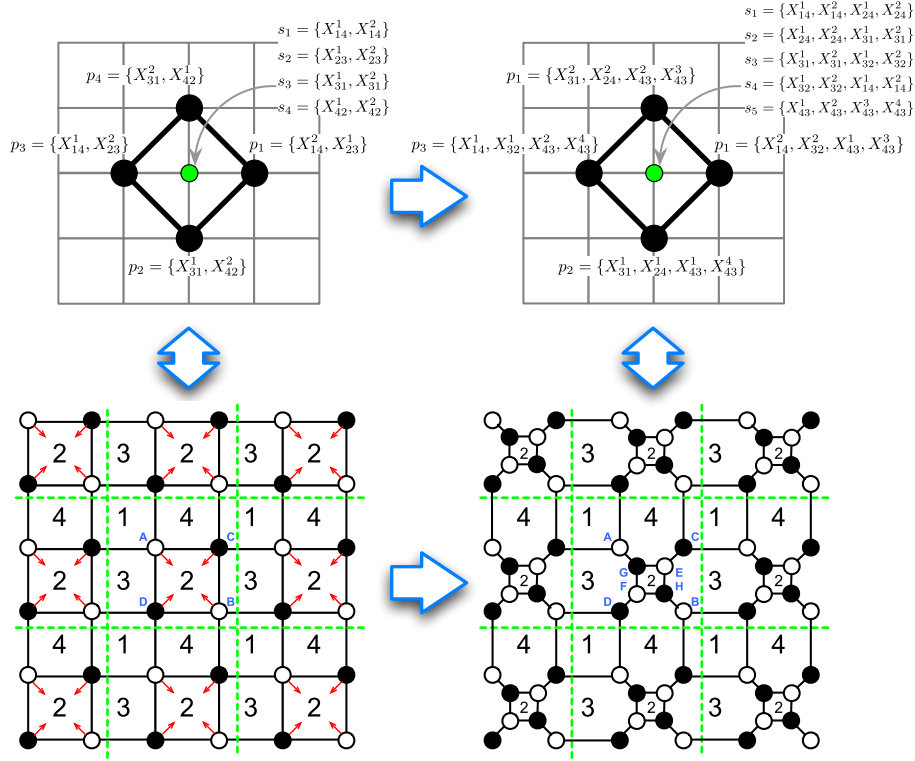


Figure 2. ‘Urban Renewal’. Toric duality acts on the brane tiling of the zeroth Hirzebruch surface F_0 . The points in the toric diagram correspond to perfect matchings and GLSM fields. Perfect matchings are defined as sets of quiver fields.

3.1 Toric Duality and Specular Duality

Toric Duality. Two $4d$ quiver gauge theories with brane tilings are called toric dual [10–16] if in the UV they have different Lagrangians with a different field content and superpotential, but flow to the same universality class in the IR.

Let us summarise the properties of toric duality for brane tilings:

- The *mesonic moduli spaces* \mathcal{M}^{mes} are the same, but the master spaces $\text{Irr } \mathcal{F}^b$ are not [48]. The mesonic Hilbert series are the same up to a fugacity map.
- The *toric diagrams* of \mathcal{M}^{mes} are $GL(2, \mathbb{Z})$ equivalent. However, multiplicities of internal toric points with zero R-charge can differ.
- The number of *gauge groups* G remains constant.

Example. The Hirzebruch \mathbb{F}_0 model has the superpotential

$$W_I = \underbrace{X_{14}^1 X_{42}^1 X_{23}^1 X_{31}^1}_A + \underbrace{X_{14}^2 X_{42}^2 X_{23}^2 X_{31}^2}_B - \underbrace{X_{14}^2 X_{42}^1 X_{23}^2 X_{31}^1}_C - \underbrace{X_{14}^1 X_{42}^2 X_{23}^1 X_{31}^2}_D, \quad (3.1)$$

with the corresponding brane tiling and toric diagram shown in the left panel of Figure 2. By dualizing on the gauge group $U(N)_2$, the superpotential becomes

$$\begin{aligned} W_{II} = & \underbrace{X_{14}^1 X_{43}^1 X_{31}^1}_A + \underbrace{X_{14}^2 X_{43}^2 X_{31}^2}_B - \underbrace{X_{14}^2 X_{43}^3 X_{31}^1}_C - \underbrace{X_{14}^1 X_{43}^4 X_{31}^2}_D \\ & + \underbrace{X_{14}^1 X_{43}^3 X_{31}^2}_E + \underbrace{X_{14}^2 X_{43}^4 X_{31}^1}_F - \underbrace{X_{14}^1 X_{43}^1 X_{31}^1}_G - \underbrace{X_{14}^2 X_{43}^2 X_{31}^2}_H \end{aligned} \quad (3.2)$$

with the associated brane tiling and toric diagram shown in the right panel of Figure 2. The figure labels toric points with the associated perfect matchings.

Specular Duality. The new correspondence has the following properties for dual brane tilings:

- $\text{Irr } \mathcal{F}^\flat$ are isomorphic⁴ and the Hilbert series are the same up to a fugacity map.
- Except for self-dual cases, \mathcal{M}^{mes} are not the same.
- The number of gauge groups G remains invariant.
- The number of matter fields E remains invariant.

There are 16 reflexive toric diagrams. They are summarized in Figure 3 [17] and relate to 30 brane tilings. Specular duality exhibits additional properties for this set of brane tilings:

- Internal/external perfect matchings of brane tiling A become external/internal perfect matchings of the dual brane tiling B.
- The mesonic flavour symmetries of brane tiling A become the anomalous or enhanced hidden baryonic symmetries of brane tiling B.

⁴Note: Specular duality extends to the full master space \mathcal{F}^\flat . We restrict the discussion to its largest component $\text{Irr } \mathcal{F}^\flat$.

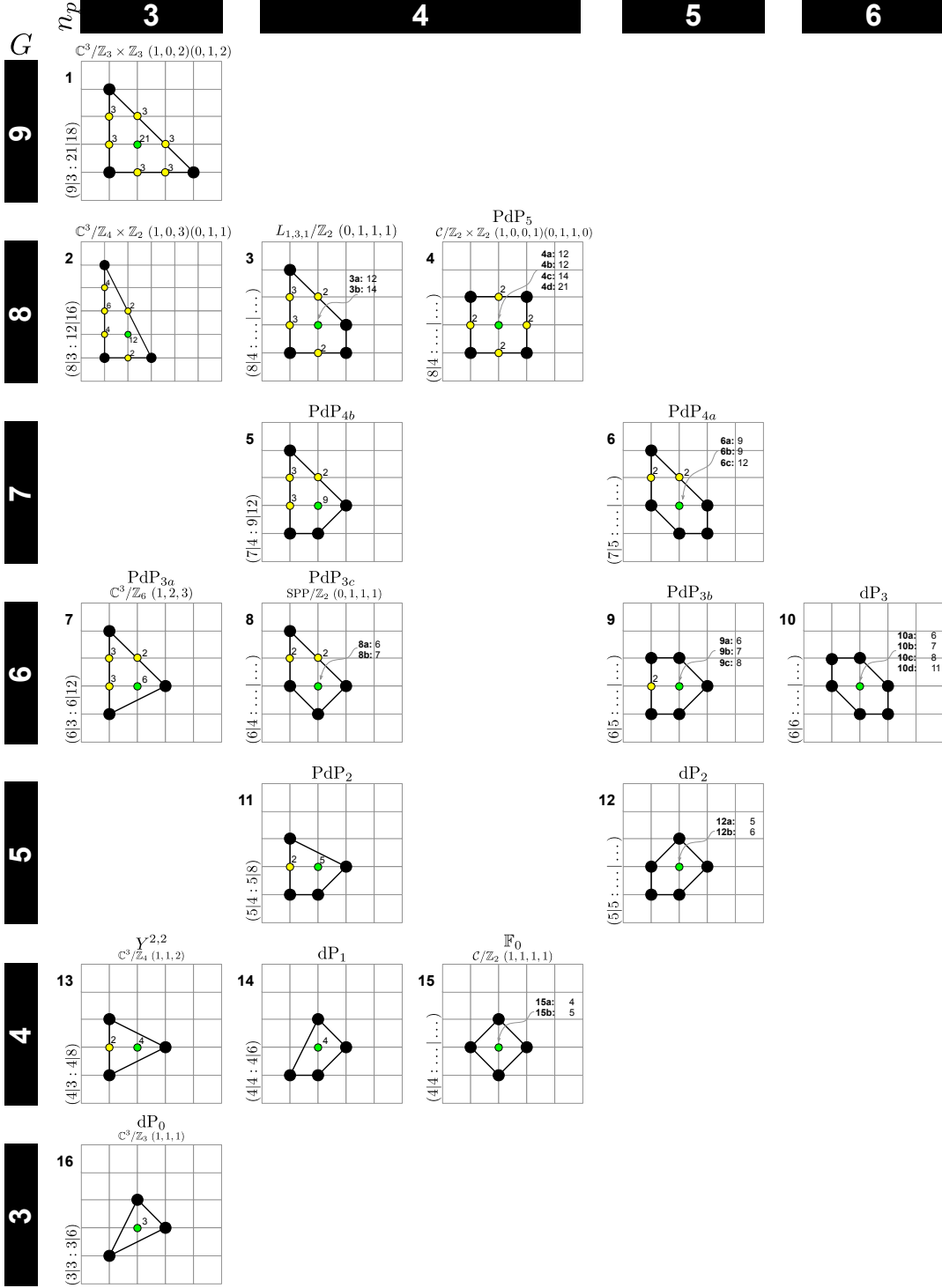


Figure 3. *Reflexive Toric Diagrams.* The figure shows the 16 reflexive toric diagrams which correspond to 30 brane tilings. Each polygon is labelled by $(G|n_p : n_i|n_W)$, where G is the number of $U(N)$ gauge groups, n_p is the number of extremal perfect matchings, n_i is the number of internal perfect matchings, and n_W is the number of superpotential terms. A reflexive polygon can correspond to multiple brane tilings by toric duality.

d	Number of Polytopes
1	1
2	16
3	4319
4	473800776

Table 1. *Counting Reflexive Polytopes.* Number of distinct reflexive lattice polytopes in dimension $d \leq 4$. The number of polytopes forms a sequence which has the OEIS identifier A090045.

As noted above, specular duality exhibits additional properties for brane tilings with reflexive toric diagrams. Many of the 30 brane tilings which correspond to the 16 reflexive polygons are toric duals [17].

Reflexive polytopes have the following properties:

- A **reflexive polytope** is a convex \mathbb{Z}^d lattice polytope whose unique interior point is the origin $(0, \dots, 0)$.
- A **dual (polar) polytope** exists for every reflexive polytope Δ . The dual Δ° is another lattice polytope with points

$$\Delta^\circ = \{v^\circ \in \mathbb{Z}^d \mid \langle v^\circ, v \rangle \geq -1 \ \forall v \in \Delta\} \quad (3.3)$$

Δ° is another reflexive polytope. There are self-dual polytopes, $\Delta = \Delta^\circ$.⁵

- A **classification of reflexive polytopes** [26–28] is available for the dimensions $d \leq 4$ as shown in Table 1.

Specular duality preserves the reflexivity of the toric diagram and the set of 30 brane tilings in Figure 3:

$$\begin{aligned}
& 1 \leftrightarrow 1 \\
& 2 \leftrightarrow 4d, \ 3a \leftrightarrow 4c, \ 3b \leftrightarrow 3b, \ 4a \leftrightarrow 4a, \ 4b \leftrightarrow 4b \\
& 5 \leftrightarrow 6c, \ 6a \leftrightarrow 6a, \ 6b \leftrightarrow 6b \\
& 7 \leftrightarrow 10d, \ 8a \leftrightarrow 10c, \ 8b \leftrightarrow 9c, \ 9a \leftrightarrow 10b, \ 9b \leftrightarrow 9b, \ 10a \leftrightarrow 10a \\
& 11 \leftrightarrow 12b, \ 12a \leftrightarrow 12a \\
& 13 \leftrightarrow 15b, \ 14 \leftrightarrow 14, \ 15a \leftrightarrow 15a \\
& 16 \leftrightarrow 16
\end{aligned} \quad . \quad (3.4)$$

⁵Note that this duality between reflexive polytopes does not correspond to specular duality.

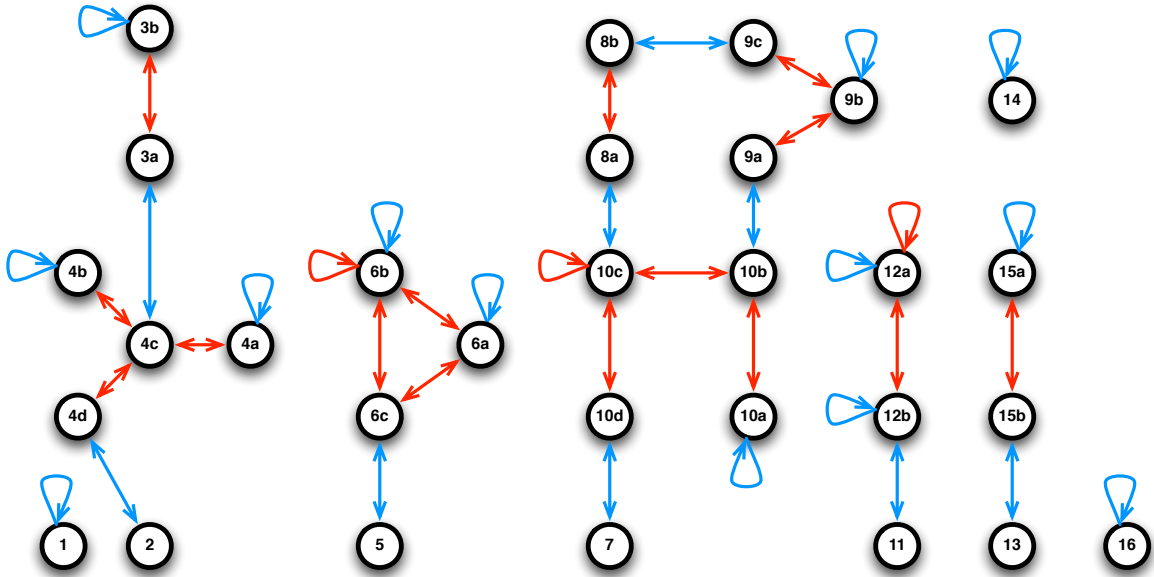


Figure 4. *Toric and Specular Duality.* These are the duality trees of brane tilings (nodes) with reflexive toric diagrams. The brane tiling labels are taken from [17] and Figure 3. Arrows indicate toric duality (red) and specular duality (blue).

Figure 5 shows the reflexive toric diagrams with specular dual brane tilings.

Self-dual Brane Tilings. Certain brane tilings with reflexive toric diagrams are self-dual. These are:

$$1, 3b, 4a, 4b, 6a, 6b, 9b, 10a, 12a, 14, 15a, 16, \quad (3.5)$$

which are summarized in Figure 6. The toric diagram and brane tiling are invariant under specular duality.

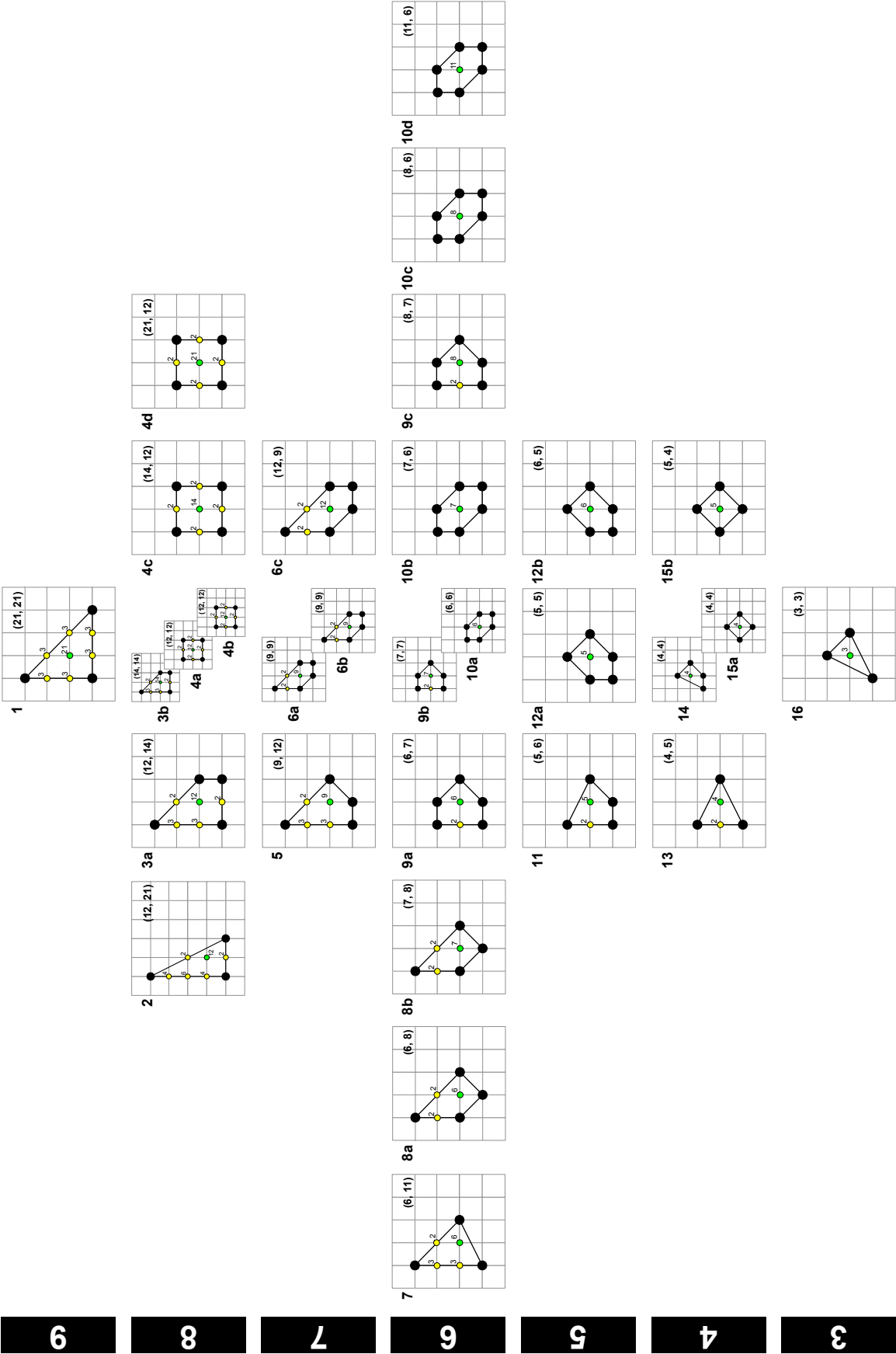
G 

Figure 5. *Arbor specularis*. The 30 reflexive toric diagrams with perfect matching multiplicities. The models are labelled with (n_i, n_e) , where n_i and n_e are the number of internal and external perfect matchings respectively. The y -axis is labelled by the number of gauge groups G or the area of the polygon, and the position along the x -axis relates to the difference $n_i - n_e$.

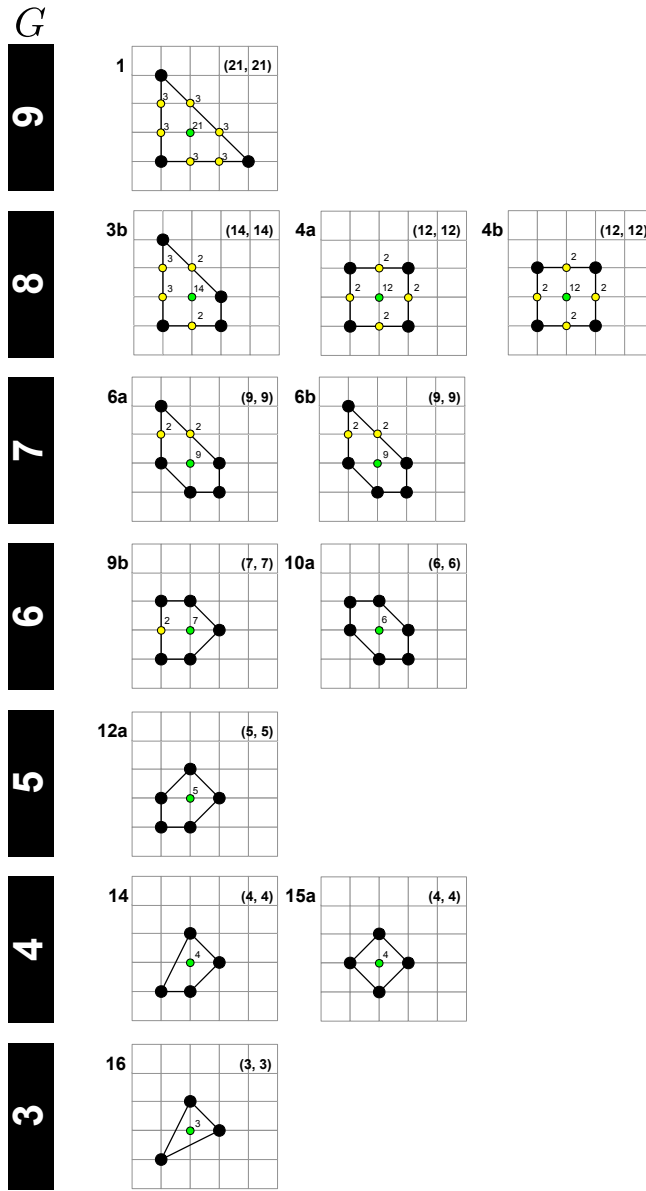


Figure 6. *Self-duals under Specular Duality.* These are the 12 reflexive toric diagrams which have self-dual brane tilings. The models are labelled with (n_i, n_e) , where n_i and n_e are the number of internal and external perfect matchings respectively.

3.2 Specular Duality and ‘Fixing’ Shivers

As illustrated in Section §3.1, toric duality has a natural interpretation on the brane tiling. The following section identifies the interpretation of specular duality on the brane tiling.

A toric singularity has an associated **characteristic polynomial**, also known as the Newton polynomial,

$$P(w, z) = \sum_{(n_1, n_2) \in \Delta} a_{n_1, n_2} w^{n_1} z^{n_2} \quad , \quad (3.6)$$

where the sum runs over all points in the toric diagram, and a_{n_1, n_2} is a complex number. The geometric description of the **mirror manifold** [34, 49, 50] is

$$\begin{aligned} Y &= P(w, z) \quad , \\ Y &= uv \quad , \end{aligned} \quad (3.7)$$

where $w, z \in \mathbb{C}^*$ and $u, v \in \mathbb{C}$. The curve $P(w, z) - Y = 0$ describes a punctured **Riemann surface** Σ_Y with

- the genus g corresponding to the number I of internal toric points
- the number of punctures corresponding to the number E of external toric points.

The Riemann surface is fibered over each point in Y . Of particular interest to us is the Riemann surface Σ fibered over the origin $Y = 0$. It is related to the brane tiling on \mathbb{T}^2 under the **untwisting map** ϕ_u [34–36].

A brane tiling consists of **zig-zag paths** η_i [21, 51]. These are collections of edges in the tiling that form closed non-trivial paths on \mathbb{T}^2 . Zig-zag paths maximally turn left at a black node and then maximally turn right at the next adjacent white node. The **winding numbers** (p, q) of zig-zag paths relate to the \mathbb{Z}^2 direction of the corresponding leg in the (p, q) -web [52]. The dual of the (p, q) -web is the toric diagram. By thickening the (p, q) -web, one obtains the punctured Riemann surface Σ .

The untwisting map ϕ_u has the following action on the brane tiling:

$$\begin{aligned} \phi_u : \quad & \text{brane tiling on } \mathbb{T}^2 \rightarrow \text{shiver on } \Sigma \\ & \text{zig-zag path } \eta_i \mapsto \text{puncture } \gamma_i \\ & \text{face/gauge group } U(N)_a \mapsto \text{zig-zag path } \tilde{\eta}_a \\ & \text{node/term } w_k, b_k \mapsto \text{node/term } w_k, b_k \\ & \text{edge/field } X_{ab} \mapsto \text{edge/field } X_{ij} \quad , \end{aligned} \quad (3.8)$$

where a, b count $U(N)$ gauge groups/brane tiling faces, i, j count zig-zag paths on the original brane tiling on \mathbb{T}^2 , and $\tilde{\eta}_a$ are zig-zag paths of the shiver on Σ . An illustration of the untwisting map is in Figure 7.

brane tiling on \mathbb{T}^2	$\xrightarrow{\phi_u}$	shiver on Σ
zig-zag path η_i	\mapsto	puncture γ_i
face/gauge group $U(N)_a$	\mapsto	zig-zag path $\tilde{\eta}_a$
node/term w_k, b_k	\mapsto	node/term w_k, b_k
edge/field X_{ab}	\mapsto	edge/field X_{ij}

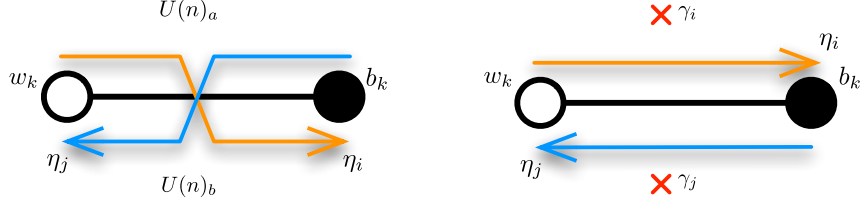


Figure 7. *The Untwisting Map ϕ_u .* The untwisting map relates a brane tiling on \mathbb{T}^2 to a shiver on a punctured Riemann surface Σ .

The untwisted brane tiling on Σ is known as a **shiver** [37–39]. It is not associated to a quiver, a superpotential and a field theory moduli space, and therefore can be interpreted as a ‘pseudo-brane tiling’ on a punctured Riemann surface. An interesting question to ask at this point is whether a shiver can be ‘fixed’ by a map ϕ_f such that it becomes a consistent brane tiling.

The main obstructions are the punctures of Σ which have no interpretation in the quiver gauge theory context. Let the punctures therefore be identified with $U(N)$ gauge groups under the following definition of the **shiver fixing map**:

$$\begin{aligned} \phi_f : \quad & \text{shiver on } \Sigma \rightarrow \text{brane tiling on } \Sigma \\ & \text{puncture } \gamma_i \mapsto \text{face/gauge group } U(N)_i \quad , \end{aligned} \quad (3.9)$$

with the zig-zag paths $\tilde{\eta}_a$, nodes w_k and b_k , and edges X_{ij} on the shiver remaining invariant.

Accordingly, using the shiver fixing map ϕ_f and the untwisting map ϕ_u , **specular duality** on brane tilings can be defined as follows

$$\begin{aligned} \phi_{\text{specular}} = \phi_f \circ \phi_u : \quad & \text{brane tiling A on } \mathbb{T}^2 \rightarrow \text{brane tiling B on } \Sigma \\ & \text{zig-zag path } \eta_i \mapsto \text{face/gauge group } U(N)_i \\ \text{face/gauge group } U(N)_a \mapsto & \text{zig-zag path } \tilde{\eta}_a \\ \text{node/term } w_k, b_k \mapsto & \text{node/term } w_k, b_k \\ \text{edge/field } X_{ab} \mapsto & \text{edge/field } X_{ij} \quad , \end{aligned} \quad (3.10)$$

where ϕ_{specular} is invertible. A graphical illustration of ϕ_{specular} is in Figure 8.

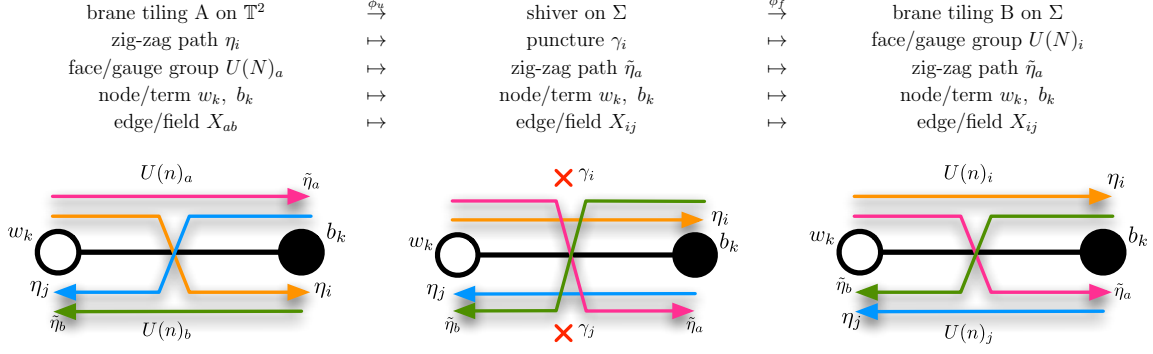


Figure 8. *Specular Duality on a Brane Tiling.* The map $\phi_{\text{specular}} = \phi_f \circ \phi_u$ which defines specular duality first untwists a brane tiling and then replaces punctures with $U(N)$ gauge groups.

For a brane tiling to have a Calabi-Yau 3-fold as its mesonic moduli space and to have a known AdS dual [23, 31, 32], it needs to be on \mathbb{T}^2 . Brane tilings with reflexive toric diagrams have a specular dual which is always on $\Sigma = \mathbb{T}^2$. This is because, as we recall, reflexive toric diagrams always have by definition $I = 1$ and their (p, q) -web has therefore always genus $g = 1$.

Invariance of the master space $\text{Irr } \mathcal{F}^\dagger$. Specular duality has an important effect on a brane tiling's superpotential W which can be demonstrated with the following example

$$W = \dots + ABC - ADE + \dots \quad , \quad (3.11)$$

where A, \dots, E are quiver fields.⁶ The corresponding nodes in the brane tiling are illustrated along with zig-zag paths in the left panel of Figure 9.

⁶There is an overall trace in the superpotential which is not written down for simplicity.

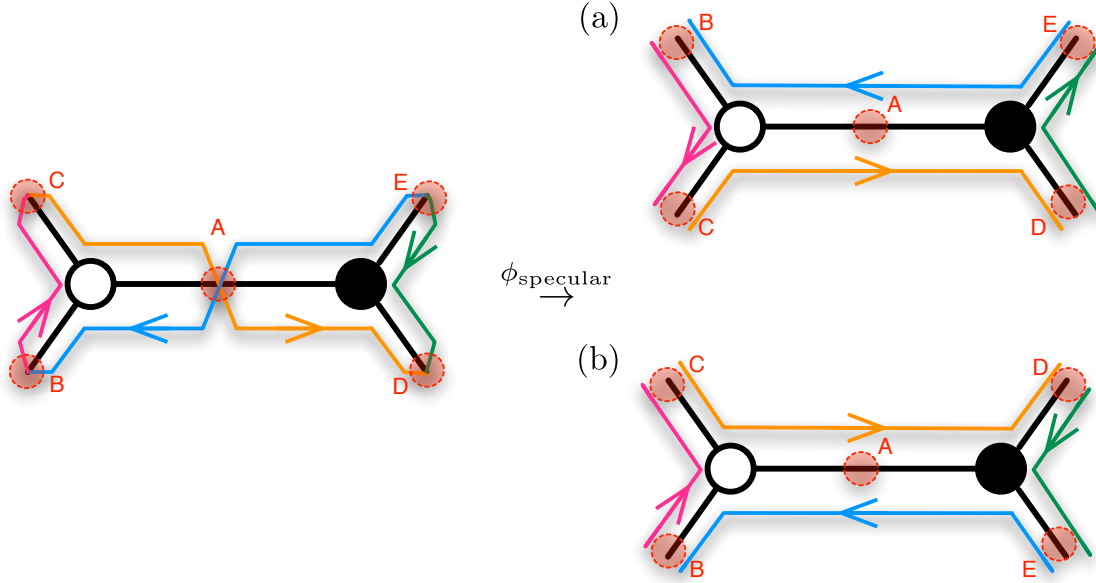


Figure 9. *Untwisting the Superpotential.* There are two equivalent ways of untwisting the brane tiling. The order of fields around either a white (clockwise) or black (anti-clockwise) node in the brane tiling is reversed under the untwisting. Either way results in the same brane tiling.

Specular duality untwists the brane tiling in such a way that the order of quiver fields around either white (clockwise) nodes or black (anti-clockwise) nodes is reversed. For the example in (3.11), the superpotential of the dual brane tiling has either the form

$$W_{(a)} = \dots + ACB - ADE + \dots \quad (3.12)$$

or the form

$$W_{(b)} = \dots + ABC - AED + \dots \quad (3.13)$$

as illustrated in the right panel of Figure 9. The options of reversing the orientation around white nodes or black nodes are equivalent up to an overall swap of node colours.

For the case of single D3 brane theories with $U(1)$ gauge groups, the fields commute such that

$$W = W_{(a)} = W_{(b)} \quad . \quad (3.14)$$

The $U(1)$ superpotential is invariant under specular duality. Since the master space $\text{Irr } \mathcal{F}^\flat$ is defined in terms of F-terms, the observation in (3.14) implies that it is invariant

under specular duality.

No specific Quiver from an Abelian W . In order to show that the master spaces of dual one brane theories are isomorphic, it is sufficient to illustrate that the superpotentials are the same when the quiver fields commute. However, it is important to note that if the cyclic order of fields in a given superpotential is not recorded, its correspondence to a specific quiver and hence a brane tiling is not unique. A simple example would be the Abelian potential for \mathbb{C}^3 or the conifold \mathcal{C} which is $W = 0$. In contrast to the distinct non-Abelian superpotentials, the trivial Abelian superpotential for these models encodes no information about the field content of the associated brane tilings.

Since specular duality is a well defined map between brane tilings, not just between Abelian superpotentials, we study in the following sections the new correspondence with the help of *characteristics of the mesonic moduli space*. An important observation is that specular duality exchanges internal and external perfect matchings for brane tilings with reflexive toric diagrams. The difference between internal and external perfect matchings is a property of the mesonic moduli space and its toric diagram.

Perfect matchings as GLSM fields are used for the symplectic quotient description of $\text{Irr } \mathcal{F}^b$. Since perfect matchings represent a choice of coordinates to identify the master space cone, one is free to introduce a new set of coordinates that correspond to the global symmetry of the field theory. In the following sections, we identify coordinate transformations that relate the exchange of internal and external perfect matchings to the exchange of mesonic flavour symmetries and hidden or anomalous baryonic symmetries. Moreover, one can find a third set of coordinates which relate to the boundaries of the Calabi-Yau cone and are used to illustrate how an exchange of internal and external perfect matchings leads to a reflection of the $\text{Irr } \mathcal{F}^b$ cone along a hyperplane.

4 Model 13 ($Y^{2,2}, \mathbb{F}_2, \mathbb{C}^3/\mathbb{Z}_4$) and Model 15b ($Y^{2,0}, \mathbb{F}_0, \mathcal{C}/\mathbb{Z}_2$)

In the following section, we study specular duality with Model 13 which is known as $Y^{2,2}, \mathbb{F}_2$ or $\mathbb{C}^3/\mathbb{Z}_4$ with action $(1, 1, 2)$ in the literature, and Model 15b which is known as phase II of $Y^{2,0}, \mathbb{F}_0$ or \mathcal{C}/\mathbb{Z}_2 with action $(1, 1, 1, 1)$.

4.1 Brane Tilings and Superpotentials

Figure 10 shows how the untwisting map ϕ_u acts on the brane tiling of Model 13 to give a shiver. The fixing map ϕ_f then takes the shiver to give the brane tiling of Model

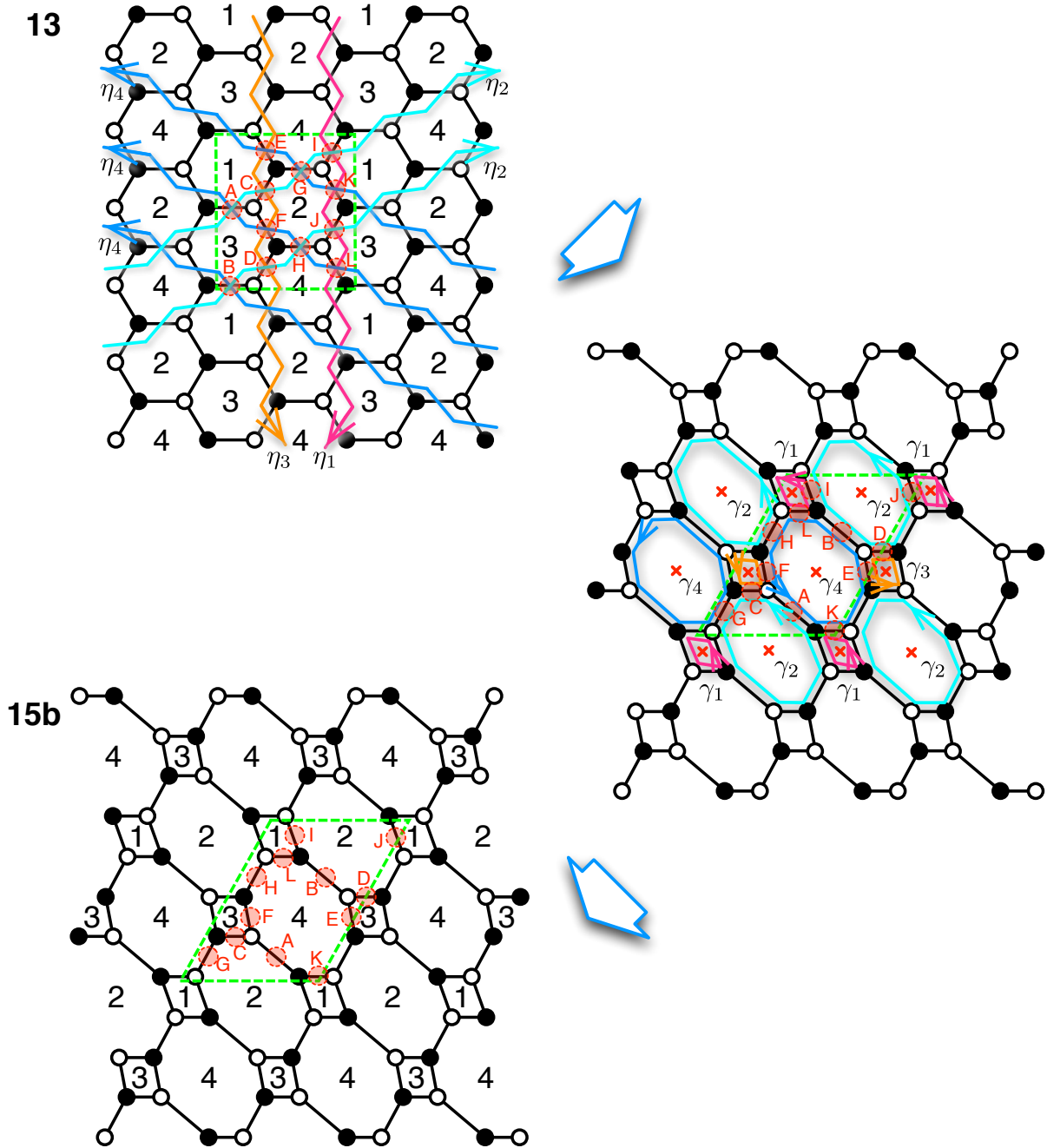


Figure 10. *Specular Duality between Models 13 and 15b.* The untwisting map ϕ_u acts on the brane tiling of Model 13 which results in a shiver. The shiver is then fixed with ϕ_f which results in the brane tiling of Model 15b.

15b. Beginning with the superpotential of Model 13,

$$\begin{aligned}
W_{13} = & +X_{12}^1 X_{24} X_{41}^1 + X_{31} X_{12}^2 X_{23}^2 + X_{41}^2 X_{13} X_{34}^1 + X_{34}^2 X_{42} X_{23}^1 \\
& - X_{12}^1 X_{23}^1 X_{31} - X_{13} X_{34}^2 X_{41}^1 - X_{41}^2 X_{12}^2 X_{24} - X_{34}^1 X_{42} X_{23}^2 \ , \quad (4.1)
\end{aligned}$$

the zig-zag paths are identified as follows

$$\begin{aligned}
\eta_1 &= \{X_{12}^1, X_{23}^1, X_{34}^2, X_{41}^1\} \ , \\
\eta_2 &= \{X_{12}^2, X_{24}, X_{41}^1, X_{13}, X_{34}^1, X_{42}, X_{23}^1, X_{31}\} \ , \\
\eta_3 &= \{X_{23}^2, X_{34}^1, X_{41}^2, X_{12}^2\} \ , \\
\eta_4 &= \{X_{13}, X_{34}^2, X_{42}, X_{23}^2, X_{31}, X_{12}^1, X_{24}, X_{41}^2\} \ . \quad (4.2)
\end{aligned}$$

The intersections of zig-zag paths highlighted in Figure 10 are

$$\begin{aligned}
(A, B, C, D, E, F, G, H, I, J, K, L) = \\
(X_{31}, X_{13}, X_{12}^2, X_{34}^1, X_{41}^2, X_{23}^2, X_{24}, X_{42}, X_{41}^1, X_{23}^1, X_{12}^1, X_{34}^2) \ . \quad (4.3)
\end{aligned}$$

Under specular duality, the intersections are mapped to the ones for zig-zag paths on the brane tiling of Model 15b.

In terms of intersections, the superpotential in (4.1) takes the form

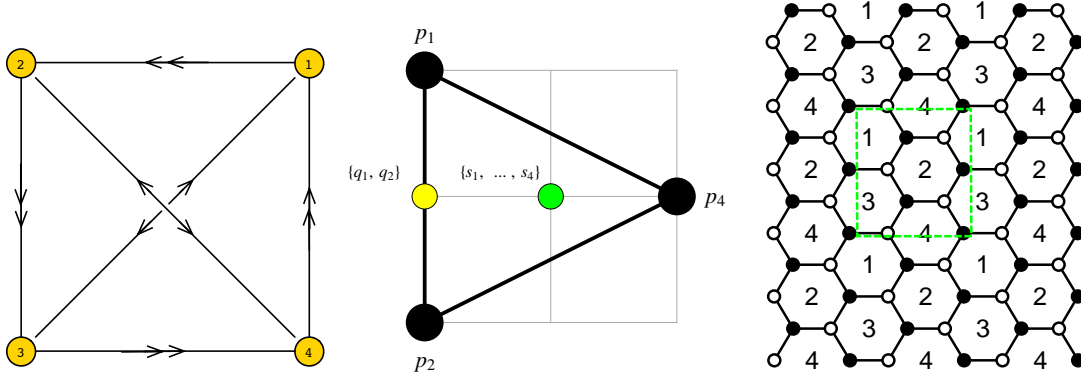
$$\begin{aligned}
W_{13} = & +KGI + ACF + EBD + LHJ \\
& -KJA - BLI - ECG - DHF \quad (4.4)
\end{aligned}$$

The intersections are also fields in the dual brane tiling of Model 15b. Accordingly, the corresponding superpotential can be written as

$$\begin{aligned}
\widetilde{W}_{13} = W_{15b} = & +X_{14}^1 X_{42}^1 X_{21}^1 + X_{42}^4 X_{23}^2 X_{34}^1 + X_{34}^2 X_{42}^3 X_{23}^1 + X_{14}^2 X_{42}^2 X_{21}^2 \\
& - X_{14}^1 X_{42}^4 X_{21}^2 - X_{42}^3 X_{21}^1 X_{14}^2 - X_{34}^2 X_{42}^1 X_{23}^2 - X_{23}^1 X_{34}^1 X_{42}^2 \\
= & +KGI + ACF + EBD + LHJ \\
& -KAJ - BIL - EGC - DFH \ . \quad (4.5)
\end{aligned}$$

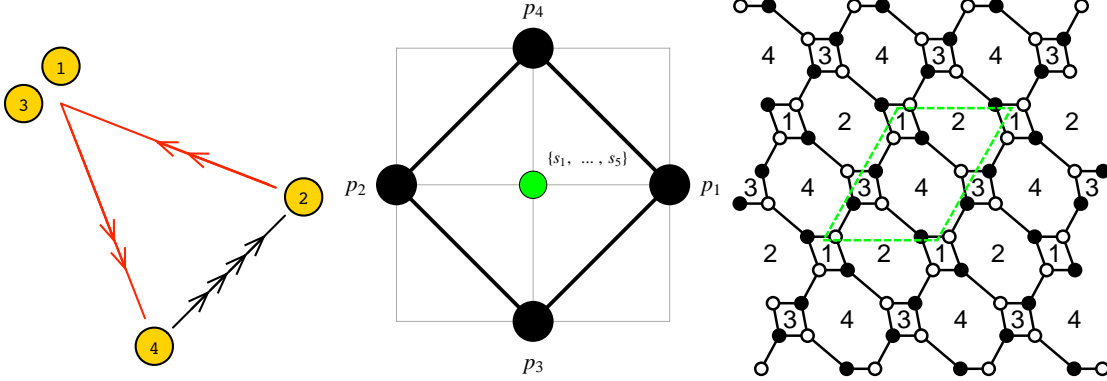
We note that the two superpotentials are the same up to a reversal of cyclic order of negative terms in (4.5). For the Abelian single D3 brane theory, the superpotentials and the corresponding F-terms are the same and hence lead to the same master space \mathcal{F}^b .

4.2 Perfect Matchings and the Hilbert Series



$$\begin{aligned}
 W_{13} = & +X_{12}^1 X_{24} X_{41}^1 + X_{31} X_{12}^2 X_{23}^2 + X_{41}^2 X_{13} X_{34}^1 + X_{34}^2 X_{42} X_{23}^1 \\
 & -X_{12}^1 X_{23}^1 X_{31} - X_{13} X_{34}^2 X_{41}^1 - X_{41}^2 X_{12}^2 X_{24} - X_{34}^1 X_{42} X_{23}^2
 \end{aligned}$$

Figure 11. The quiver, toric diagram, brane tiling and superpotential of Model 13.



$$\begin{aligned}
 W_{15b} = & +X_{14}^1 X_{42}^1 X_{21}^1 + X_{42}^4 X_{23}^2 X_{34}^1 + X_{34}^2 X_{42}^3 X_{23}^1 + X_{14}^2 X_{42}^2 X_{21}^2 \\
 & -X_{14}^1 X_{42}^4 X_{21}^2 - X_{42}^3 X_{21}^1 X_{14}^2 - X_{34}^2 X_{42}^1 X_{23}^2 - X_{23}^1 X_{34}^1 X_{42}^2
 \end{aligned}$$

Figure 12. The quiver, toric diagram, brane tiling and superpotential of Model 15b.

In order to illustrate that specular duality exchanges internal and external perfect matchings of brane tilings, we consider the symplectic quotient description of $\text{Irr } \mathcal{F}^b$. It uses GLSM fields which relate to perfect matchings in a brane tiling. They are summarized in matrices which are for Model 13 and 15b respectively

$$P^{13} = \left(\begin{array}{c|ccc|cc|cccc} & p_1 & p_2 & p_3 & q_1 & q_2 & s_1 & s_2 & s_3 & s_4 \\ \hline I = X_{41}^1 & 1 & 0 & 0 & 1 & 0 & 1 & 0 & 0 & 0 \\ E = X_{41}^2 & 0 & 1 & 0 & 1 & 0 & 1 & 0 & 0 & 0 \\ J = X_{23}^1 & 1 & 0 & 0 & 1 & 0 & 0 & 1 & 0 & 0 \\ F = X_{23}^2 & 0 & 1 & 0 & 1 & 0 & 0 & 1 & 0 & 0 \\ C = X_{12}^2 & 1 & 0 & 0 & 0 & 1 & 0 & 0 & 1 & 0 \\ K = X_{12}^1 & 0 & 1 & 0 & 0 & 1 & 0 & 0 & 1 & 0 \\ D = X_{34}^1 & 1 & 0 & 0 & 0 & 1 & 0 & 0 & 0 & 1 \\ L = X_{34}^2 & 0 & 1 & 0 & 0 & 1 & 0 & 0 & 0 & 1 \\ H = X_{42} & 0 & 0 & 1 & 0 & 0 & 1 & 0 & 1 & 0 \\ A = X_{31} & 0 & 0 & 1 & 0 & 0 & 1 & 0 & 0 & 1 \\ B = X_{13} & 0 & 0 & 1 & 0 & 0 & 0 & 1 & 1 & 0 \\ G = X_{24} & 0 & 0 & 1 & 0 & 0 & 0 & 1 & 0 & 1 \end{array} \right), \quad P^{15b} = \left(\begin{array}{c|cccc|ccccc} & p_1 & p_2 & p_3 & p_4 & s_1 & s_2 & s_3 & s_4 & s_5 \\ \hline I = X_{21}^1 & 1 & 0 & 0 & 0 & 1 & 0 & 0 & 1 & 0 \\ E = X_{34}^2 & 1 & 0 & 0 & 0 & 0 & 1 & 0 & 1 & 0 \\ J = X_{21}^2 & 0 & 1 & 0 & 0 & 1 & 0 & 0 & 1 & 0 \\ F = X_{34}^1 & 0 & 1 & 0 & 0 & 0 & 1 & 0 & 1 & 0 \\ C = X_{23}^2 & 0 & 0 & 1 & 0 & 1 & 0 & 0 & 0 & 1 \\ K = X_{14}^1 & 0 & 0 & 1 & 0 & 0 & 1 & 0 & 0 & 1 \\ D = X_{23}^1 & 0 & 0 & 0 & 1 & 1 & 0 & 0 & 0 & 1 \\ L = X_{14}^2 & 0 & 0 & 0 & 1 & 0 & 1 & 0 & 0 & 1 \\ H = X_{42}^2 & 1 & 0 & 1 & 0 & 0 & 0 & 1 & 0 & 0 \\ A = X_{42}^4 & 1 & 0 & 0 & 1 & 0 & 0 & 1 & 0 & 0 \\ B = X_{42}^3 & 0 & 1 & 1 & 0 & 0 & 0 & 1 & 0 & 0 \\ G = X_{42}^1 & 0 & 1 & 0 & 1 & 0 & 0 & 1 & 0 & 0 \end{array} \right).$$

The corresponding F-term charge matrices are

$$Q_F^{13} = \left(\begin{array}{c|ccc|cc|cccc} p_1 & p_2 & p_3 & q_1 & q_2 & s_1 & s_2 & s_3 & s_4 \\ \hline 0 & 0 & -1 & -1 & 0 & 1 & 1 & 0 & 0 \\ 0 & 0 & -1 & 0 & -1 & 0 & 0 & 1 & 1 \\ 1 & 1 & 0 & -1 & -1 & 0 & 0 & 0 & 0 \end{array} \right), \quad Q_F^{15b} = \left(\begin{array}{c|cccc|ccccc} p_1 & p_2 & p_3 & p_4 & s_1 & s_2 & s_3 & s_4 & s_5 \\ \hline 1 & 1 & 0 & 0 & 0 & 0 & -1 & -1 & 0 \\ 0 & 0 & 1 & 1 & 0 & 0 & -1 & 0 & -1 \\ 0 & 0 & 0 & 0 & 1 & 1 & 0 & -1 & -1 \end{array} \right).$$

From the quiver incidence matrices, one obtains the following D-term charge matrices

$$Q_D^{13} = \left(\begin{array}{c|ccc|cc|cccc} p_1 & p_2 & p_3 & q_1 & q_2 & s_1 & s_2 & s_3 & s_4 \\ \hline 0 & 0 & 0 & 1 & -1 & 0 & 0 & 0 & 0 \\ 0 & 0 & 0 & 0 & 0 & 1 & -1 & 0 & 0 \\ 0 & 0 & 0 & 0 & 0 & 0 & 0 & 1 & -1 \end{array} \right), \quad Q_D^{15b} = \left(\begin{array}{c|cccc|ccccc} p_1 & p_2 & p_3 & p_4 & s_1 & s_2 & s_3 & s_4 & s_5 \\ \hline 0 & 0 & 0 & 0 & 0 & 1 & -1 & 0 & 0 \\ 0 & 0 & 0 & 0 & 0 & 0 & 1 & -1 & 0 \\ 0 & 0 & 0 & 0 & 0 & 0 & 0 & 1 & -1 \end{array} \right).$$

The kernel of the total charge matrix Q_t leads to the coordinates of points in the toric diagram,

$$G_t^{13} = \left(\begin{array}{c|ccc|cc|cccc} p_1 & p_2 & p_3 & q_1 & q_2 & s_1 & s_2 & s_3 & s_4 \\ \hline 0 & 0 & 2 & 0 & 0 & 1 & 1 & 1 & 1 \\ 2 & 0 & -1 & 1 & 1 & 0 & 0 & 0 & 0 \\ 1 & 1 & 1 & 1 & 1 & 1 & 1 & 1 & 1 \end{array} \right), \quad G_t^{15b} = \left(\begin{array}{c|cccc|ccccc} p_1 & p_2 & p_3 & p_4 & s_1 & s_2 & s_3 & s_4 & s_5 \\ \hline 2 & 0 & 2 & 0 & 1 & 1 & 1 & 1 & 1 \\ 0 & 0 & -1 & 1 & 0 & 0 & 0 & 0 & 0 \\ 1 & 1 & 1 & 1 & 1 & 1 & 1 & 1 & 1 \end{array} \right).$$

Note that the corresponding toric diagrams in Figure 11 and Figure 12 are $GL(2, \mathbb{Z})$ transformed.

The columns in the G_t matrices indicate the coordinates of points in the toric diagram with the associated perfect matchings. Using this information, one relates columns of the matrices Q_F , Q_D and P to either external or internal perfect matchings.

Specular duality swaps external and internal perfect matchings as follows

$$(p_1, p_2, p_3, q_1, q_2, s_1, s_2, s_3, s_4)_{13} \leftrightarrow (s_1, s_2, s_3, s_4, s_5, p_1, p_2, p_3, p_4)_{15b} \quad . \quad (4.6)$$

Accordingly, the duality maps the perfect matching matrix P^{13} to P^{15b} as well as the F-term charge matrix Q_F^{13} to Q_F^{15b} by a swap of matrix columns. As a result, the following

symplectic quotient descriptions of the master spaces $\text{Irr } \mathcal{F}^b$ are isomorphic

$$\begin{aligned}\text{Irr } \mathcal{F}_{13}^b &= \mathbb{C}^9[p_1, p_2, p_3, q_1, q_2, s_1, s_2, s_3, s_4] // Q_F^{13} , \\ \text{Irr } \mathcal{F}_{15b}^b &= \mathbb{C}^9[p_1, p_2, p_3, p_4, s_1, s_2, s_3, s_4, s_5] // Q_F^{15b} .\end{aligned}\quad (4.7)$$

Specular duality can therefore be observed on the level of the Hilbert series of $\text{Irr } \mathcal{F}^b$. Starting with Model 15b, its symplectic quotient leads to the following refined Hilbert series

$$\begin{aligned}g_1(t_i, y_{s_i}; \text{Irr } \mathcal{F}_{15b}^b) &= \prod_{i=1}^3 \oint_{|z_i|=1} \frac{dz_i}{2\pi i z_i} \frac{1}{(1-z_1 t_1)(1-z_1 t_2)(1-z_2 t_3)(1-z_2 t_4)(1-z_3 s_1)} \\ &\quad \times \frac{1}{(1-z_3 s_2)(1-\frac{1}{z_1 z_2} s_3)(1-\frac{1}{z_1 z_3} s_4)(1-\frac{1}{z_2 z_3} s_5)} \\ &= \frac{P(t_i, y_{s_i})}{(1-t_1 t_2 y_{s_3})(1-t_2 t_3 y_{s_3})(1-t_1 t_4 y_{s_3})(1-t_2 t_4 y_{s_3})} \\ &\quad \times \frac{1}{(1-t_1 s_1 y_{s_4})(1-t_2 s_1 y_{s_4})(1-t_1 y_{s_2} y_{s_4})(1-t_2 y_{s_2} y_{s_4})} \\ &\quad \times \frac{1}{(1-t_3 y_{s_1} y_{s_5})(1-t_4 y_{s_1} y_{s_5})(1-t_3 y_{s_2} y_{s_5})(1-t_4 y_{s_2} y_{s_5})} ,\end{aligned}\quad (4.8)$$

where the numerator $P(t_i, y_{s_i})$ is presented in appendix §B. Fugacities t_i and y_{s_i} count external and internal perfect matchings p_i and s_i of Model 15b respectively. The plethystic logarithm of the Hilbert series is

$$\begin{aligned}PL[g_1(t_i, y_{s_i}; \text{Irr } \mathcal{F}_{15b}^b)] &= y_{s_1} y_{s_4} t_1 + y_{s_2} y_{s_4} t_1 + y_{s_1} y_{s_4} t_2 + y_{s_2} y_{s_4} t_2 + y_{s_1} y_{s_5} t_3 + y_{s_2} y_{s_5} t_3 \\ &\quad + y_{s_1} y_{s_5} t_4 + y_{s_2} y_{s_5} t_4 + y_{s_3} t_1 t_3 + y_{s_3} t_2 t_3 + y_{s_3} t_1 t_4 + y_{s_3} t_2 t_4 - y_{s_1} y_{s_2} y_{s_4} y_{s_5} t_1 t_3 \\ &\quad - y_{s_1} y_{s_2} y_{s_4} y_{s_5} t_2 t_3 - y_{s_1} y_{s_2} y_{s_4} y_{s_5} t_1 t_4 - y_{s_1} y_{s_2} y_{s_4} y_{s_5} t_2 t_4 - y_{s_1} y_{s_2} y_{s_4}^2 t_1 t_2 - y_{s_1} y_{s_2} y_{s_5}^2 t_3 t_4 \\ &\quad - y_{s_1} y_{s_3} y_{s_4} t_1 t_2 t_3 - y_{s_2} y_{s_3} y_{s_4} t_1 t_2 t_3 - y_{s_1} y_{s_3} y_{s_4} t_1 t_2 t_4 - y_{s_2} y_{s_3} y_{s_4} t_1 t_2 t_4 - y_{s_1} y_{s_3} y_{s_5} t_1 t_3 t_4 \\ &\quad - y_{s_2} y_{s_3} y_{s_5} t_1 t_3 t_4 - y_{s_1} y_{s_3} y_{s_5} t_2 t_3 t_4 - y_{s_2} y_{s_3} y_{s_5} t_2 t_3 t_4 - y_{s_3}^2 t_1 t_2 t_3 t_4 + \dots .\end{aligned}\quad (4.9)$$

It is not finite and therefore indicates that the master space is not a complete intersection.

By specular duality, we obtain the Hilbert series in terms of the perfect matching fugacities of Model 13. The perfect matching map in (4.6) translates to the fugacity map

$$(y_{s_i}, t_{1,2,3}, y_{q_{1,2}})_{13} \leftrightarrow (t_i, y_{s_{1,2,3}}, y_{s_{4,5}})_{15b} ,\quad (4.10)$$

where $(y_{s_i}, t_{1,2,3}, y_{q_{1,2}})$ are the fugacities for perfect matchings $(s_i, t_{1,2,3}, q_{1,2})$ of Model 13 respectively.

4.3 Global Symmetries and the Hilbert Series

In order to discuss global symmetries, let us introduce the notation of subscripts and superscripts on groups which refer to fugacities and model numbers respectively.

The F-term charge matrix for Model 13 indicates that the global symmetry is $SU(2)_x^{[13]} \times U(1)_f^{[13]} \times SU(2)_{h_1}^{[13]} \times SU(2)_{h_2}^{[13]} \times U(1)_b^{[13]} \times U(1)_R^{[13]}$, where $SU(2)_x^{[13]} \times U(1)_f^{[13]} \times U(1)_R^{[13]}$ represents the mesonic symmetry, $SU(2)_{h_1}^{[13]} \times SU(2)_{h_2}^{[13]}$ the hidden baryonic symmetry, and $U(1)_b^{[13]}$ the remaining baryonic symmetry. In comparison, for Model 15b, where internal and external perfect matchings are swapped under specular duality, the global symmetry is $SU(2)_x^{[15b]} \times SU(2)_y^{[15b]} \times SU(2)_{h_1}^{[15b]} \times U(1)_{h_2}^{[15b]} \times U(1)_b^{[15b]} \times U(1)_R^{[15b]}$. The mesonic symmetry is $SU(2)_x^{[15b]} \times SU(2)_y^{[15b]} \times U(1)_R^{[15b]}$, the hidden baryonic symmetry is $SU(2)_{h_1}^{[15b]} \times U(1)_{h_2}^{[15b]}$, and the remaining baryonic symmetry is $U(1)_b^{[15b]}$.

Accordingly, we observe that the swap of external and internal perfect matchings under specular duality leads to the following correspondence between global symmetries

$$\begin{aligned}
 SU(2)_x^{[13]} \times U(1)_f^{[13]} &\leftrightarrow SU(2)_{h_1}^{[15b]} \times U(1)_{h_2}^{[15b]} \\
 SU(2)_{h_1}^{[13]} \times SU(2)_{h_2}^{[13]} &\leftrightarrow SU(2)_x^{[15b]} \times SU(2)_y^{[15b]} \\
 U(1)_b^{[13]} &\leftrightarrow U(1)_b^{[15b]} .
 \end{aligned} \tag{4.11}$$

It is a swap between mesonic flavour and hidden baryonic symmetries.

Following the discussion in appendix §A, one can find global charges on perfect matchings such that the swap of external and internal perfect matchings corresponds to a swap of mesonic flavor and hidden baryonic symmetry charges. A choice of such perfect matching charges for Model 13 and Model 15b is in Table 2 and Table 3 respectively.

	$SU(2)_x$	$U(1)_f$	$SU(2)_{h_1}$	$SU(2)_{h_2}$	$U(1)_b$	$U(1)_R$	fugacity
p_1	+1	+1	0	0	0	2/3	t_1
p_2	-1	+1	0	0	0	2/3	t_2
p_3	0	-2	0	0	0	2/3	t_3
q_1	0	0	0	0	+1	0	y_{q_1}
q_2	0	0	0	0	-1	0	y_{q_2}
s_1	0	0	+1	0	0	0	y_{s_1}
s_2	0	0	-1	0	0	0	y_{s_2}
s_3	0	0	0	+1	0	0	y_{s_3}
s_4	0	0	0	-1	0	0	y_{s_4}

Table 2. Perfect matchings of Model 13 with global charge assignment.

	$SU(2)_x$	$SU(2)_y$	$SU(2)_{h_1}$	$U(1)_{h_2}$	$U(1)_b$	$U(1)_R$	fugacity
p_1	+1	0	0	0	0	1/2	t_1
p_2	-1	0	0	0	0	1/2	t_2
p_3	0	+1	0	0	0	1/2	t_3
p_4	0	-1	0	0	0	1/2	t_4
s_1	0	0	+1	+1	0	0	y_{s_1}
s_2	0	0	-1	+1	0	0	y_{s_2}
s_3	0	0	0	-2	0	0	y_{s_3}
s_4	0	0	0	0	+1	0	y_{s_4}
s_5	0	0	0	0	-1	0	y_{s_5}

Table 3. Perfect matchings of Model 15b with global charge assignment.

Starting from Model 15b, the following fugacity map

$$\begin{aligned}
t &= (y_{s_1} y_{s_2} y_{s_3} y_{s_4} y_{s_5} t_1 t_2 t_3 t_4)^{1/4}, \quad x = t_1^{1/2} t_2^{-1/2}, \quad y = t_3^{1/2} t_4^{-1/2}, \\
b &= (y_{s_4} y_{s_5})^{1/2} (t_1 t_2)^{1/4} (t_3 t_4)^{-1/4}, \quad h_1 = y_{s_1}^{1/2} y_{s_2}^{-1/2}, \quad h_2 = (y_{s_1} y_{s_2} y_{s_4} y_{s_5})^{1/4} y_{s_3}^{-1/4},
\end{aligned} \tag{4.12}$$

leads to the refined Hilbert series in (4.8) and the corresponding plethystic logarithm in (4.9) in terms of characters of irreducible representations of the global symmetry. The expansion of the Hilbert series takes the form

$$\begin{aligned}
g_1(t, x, y, h_i, b; \text{Irr } \mathcal{F}_{15b}^\flat) &= \\
&\sum_{n_1=0}^{\infty} \sum_{n_2=0}^{\infty} \sum_{n_3=0}^{\infty} h_2^{n_1+n_2-2n_3} b^{-n_1+n_2} [n_2+n_3; n_1+n_3; n_1+n_2] t^{n_1+n_2+2n_3},
\end{aligned} \tag{4.13}$$

where $[n_1; n_2; n_3] \equiv [n_1]_x [n_2]_y [n_3]_{h_1}$ is the combined character of representations of $SU(2)_x \times SU(2)_y \times SU(2)_{h_1}$.⁷ The corresponding plethystic logarithm is

$$\begin{aligned}
PL[g_1(t, x, y, h_i, b; \text{Irr } \mathcal{F}_{15b}^\flat)] &= [1; 0; 1] h_2 b t + [0; 1; 1] h_2 b^{-1} t + [1; 1; 0] h_2^{-2} t^2 \\
&\quad - [1; 1; 0] h_2^2 t^2 - [1; 0; 1] h_2^{-1} b^{-1} t^3 - [0; 1; 1] h_2^{-1} b t^3 \\
&\quad - h_2^2 b^2 t^2 - h_2^2 b^{-2} t^2 - h_2^{-4} t^4 + \dots \quad .
\end{aligned} \tag{4.14}$$

⁷cf. [48] with a choice of charges on fields which relates to the choice presented here. The identification $F_1 = SU(2)_x$, $F_2 = SU(2)_y$, $A_2 = SU(2)_{h_1}$, $A_1 = U(1)_{h_2}$, $B = U(1)_b$ and $R = U(1)_R$ is made.

In comparison, in terms of global charges on perfect matchings of Model 13, the fugacity map

$$\begin{aligned}
t &= (y_{s_1} y_{s_2} y_{s_3} y_{s_4} y_{q_1} y_{q_2} t_1 t_2 t_3)^{1/3} , \quad x = t_1^{1/2} t_2^{-1/2} , \\
f &= (y_{s_1} y_{s_2} y_{s_3} y_{s_4})^{-1/12} (y_{q_1} y_{q_2} t_1 t_2)^{1/6} t_3^{-1/3} , \\
h_1 &= y_{s_1}^{1/2} y_{s_2}^{-1/2} , \quad h_2 = y_{s_3}^{1/2} y_{s_4}^{-1/2} , \\
b &= (y_{s_1} y_{s_2})^{1/4} (y_{s_3} y_{s_4})^{-1/4} y_{q_1}^{1/2} y_{q_2}^{-1/2} ,
\end{aligned} \tag{4.15}$$

leads to the following Hilbert series

$$\begin{aligned}
g_1(t, x, f, h_i, b; \text{Irr } \mathcal{F}_{13}^\dagger) &= \\
&\sum_{n_1=0}^{\infty} \sum_{n_2=0}^{\infty} \sum_{n_3=0}^{\infty} f^{n_1+n_2-2n_3} b^{-n_1+n_2} [n_1+n_2; n_2+n_3; n_1+n_3] t^{n_1+n_2+n_3} ,
\end{aligned} \tag{4.16}$$

where $[n_1; n_2; n_3] \equiv [n_1]_x [n_2]_{h_1} [n_3]_{h_2}$ is the combined character of representations of $SU(2)_x \times SU(2)_{h_1} \times SU(2)_{h_2}$.

The $U(1)_R$ charges on perfect matchings of Model 15b are not mapped by specular duality to $U(1)_R$ charges on perfect matchings of Model 13. This is mainly because only extremal perfect matchings carry non-zero R-charges. In order to illustrate specular duality in terms of the refined Hilbert series, one can without losing track of the algebraic structure of the moduli space mix the $U(1)_R$ symmetry with the remaining symmetry. This effectively modifies the charge assignment under the global symmetry.⁸ The modification is done via the fugacity map

$$\begin{aligned}
\tilde{t} &= (y_{s_1} y_{s_2} y_{s_3} y_{s_4} y_{q_1} y_{q_2} t_1 t_2 t_3)^{1/4} , \quad x = t_1^{1/2} t_2^{-1/2} , \\
\tilde{f} &= (y_{q_1} y_{q_2} t_1 t_2)^{1/4} t_3^{-1/4} , \\
h_1 &= y_{s_1}^{1/2} y_{s_2}^{-1/2} , \quad h_2 = y_{s_3}^{1/2} y_{s_4}^{-1/2} , \\
b &= (y_{s_1} y_{s_2})^{1/4} (y_{s_3} y_{s_4})^{-1/4} y_{q_1}^{1/2} y_{q_2}^{-1/2} ,
\end{aligned} \tag{4.17}$$

which leads to the Hilbert series

$$\begin{aligned}
g_1(\tilde{t}, x, f, h_i, b; \text{Irr } \mathcal{F}_{13}^\dagger) &= \\
&\sum_{n_1=0}^{\infty} \sum_{n_2=0}^{\infty} \sum_{n_3=0}^{\infty} \tilde{f}^{n_1+n_2-2n_3} b^{-n_1+n_2} [n_1+n_2; n_2+n_3; n_1+n_3] \tilde{t}^{n_1+n_2+2n_3} ,
\end{aligned} \tag{4.18}$$

⁸The algebraic structure of the moduli space is not lost when the orthogonality of global charges on perfect matchings is preserved as discussed in appendix §A.

where $[n_1; n_2; n_3] \equiv [n_1]_x [n_2]_{h_1} [n_3]_{h_2}$. One observes that the fugacity map equivalent to the exchange of mesonic flavour and hidden baryonic symmetries is

$$(x, \tilde{f}, \tilde{t}, h_1, h_2, b)_{13} \leftrightarrow (h_1, h_2, t, x, y, b)_{15b} \quad . \quad (4.19)$$

It relates the Hilbert series in (4.13) to the one in (4.18).

4.4 Generators, the Master Space Cone and the Hilbert Series

The master space is toric Calabi-Yau and has a conical structure. Since the dimension of the master space is $G + 2 = 6$, the corresponding Hilbert series can be rewritten in terms of 6 fugacities T_i such that the exponents of T_i are positive only. This means that all elements of the ring and the corresponding integral points of the moduli space cone relate to monomials of the form $\prod_i T_i^{m_i}$ with $m_i \geq 0$ in the Hilbert series expansion. The appropriate interpretation for these monomials is that if b T_i vanish in $\prod_i T_i^{m_i}$, the associated integral point is on a codimension b cone. All points associated to monomials $\prod_i T_i^{m_i}$ with $m_i > 0$ for all i lie within the codimension 0 cone. The boundary of the codimension 0 cone is defined by monomials of the form $T_i^{m_i}$ with $m_i > 0$.

Starting with the perfect matchings of Model 15b, the fugacity map

$$\begin{aligned} T_1 &= x = t_1^{1/2} t_2^{-1/2} \quad , \quad T_2 = y = t_3^{1/2} t_4^{-1/2} \quad , \\ T_3 &= b = (y_{s_4} y_{s_5})^{1/2} (t_1 t_2)^{1/4} (t_3 t_4)^{-1/4} \quad , \\ T_4 &= h_1 = y_{s_1}^{1/2} y_{s_2}^{-1/2} \quad , \quad T_5 = h_2 = (y_{s_1} y_{s_2} y_{s_5})^{1/4} y_{s_3}^{-1/4} \quad , \\ T_6 &= \frac{t}{x y b h_1 h_2} = (y_{s_1} y_{s_2} y_{s_3} y_{s_4} y_{s_5} t_1 t_2 t_3 t_4)^{1/4} \quad , \end{aligned} \quad (4.20)$$

allows us to re-write the Hilbert series such that the corresponding plethystic logarithm in (4.9) takes the form

$$\begin{aligned} PL[g(T_i; \text{Irr } \mathcal{F}_{15b}^b)] &= T_1^2 T_2 T_3^2 T_4^2 T_5^2 T_6 + T_1^2 T_2 T_3^2 T_5^2 T_6 + T_2 T_3^2 T_4^2 T_5^2 T_6 + T_2 T_3^2 T_5^2 T_6 \\ &+ T_1 T_2^2 T_4^2 T_5^2 T_6 + T_1 T_2^2 T_5^2 T_6 + T_1 T_4^2 T_5^2 T_6 + T_1 T_5^2 T_6 + T_1^3 T_2^3 T_3^2 T_4^2 T_6^2 + T_1 T_2^3 T_3^2 T_4^2 T_6^2 \\ &+ T_1^3 T_2 T_3^2 T_4^2 T_6^2 + T_1 T_2 T_3^2 T_4^2 T_6^2 - T_1^3 T_2^3 T_3^2 T_4^2 T_5^4 T_6^2 - T_1 T_2^3 T_3^2 T_4^2 T_5^4 T_6^2 \\ &- T_1^3 T_2 T_3^2 T_4^2 T_5^4 T_6^2 - T_1 T_2 T_3^2 T_4^2 T_5^4 T_6^2 - T_1^2 T_2^2 T_3^4 T_4^2 T_5^4 T_6^2 - T_1^2 T_2^2 T_4^2 T_5^4 T_6^2 \\ &- T_1^3 T_2^4 T_3^4 T_4^2 T_5^2 T_6^3 - T_1^3 T_2^4 T_3^4 T_4^2 T_5^2 T_6^3 - T_1^3 T_2^3 T_3^4 T_4^2 T_5^2 T_6^3 - T_1^3 T_2^2 T_3^4 T_4^2 T_5^2 T_6^3 \\ &- T_1^4 T_2^3 T_3^2 T_4^2 T_5^2 T_6^3 - T_1^4 T_2^3 T_3^2 T_4^2 T_5^2 T_6^3 - T_1^2 T_2^3 T_3^2 T_4^2 T_5^2 T_6^3 - T_1^2 T_2^3 T_3^2 T_4^2 T_5^2 T_6^3 \\ &- T_1^4 T_2^4 T_3^4 T_4^4 T_6^4 + \dots \quad . \end{aligned} \quad (4.21)$$

As desired, the plethystic logarithm as for the Hilbert series is such that the exponents of the fugacities T_i are positive. In comparison, in relation to perfect matchings of

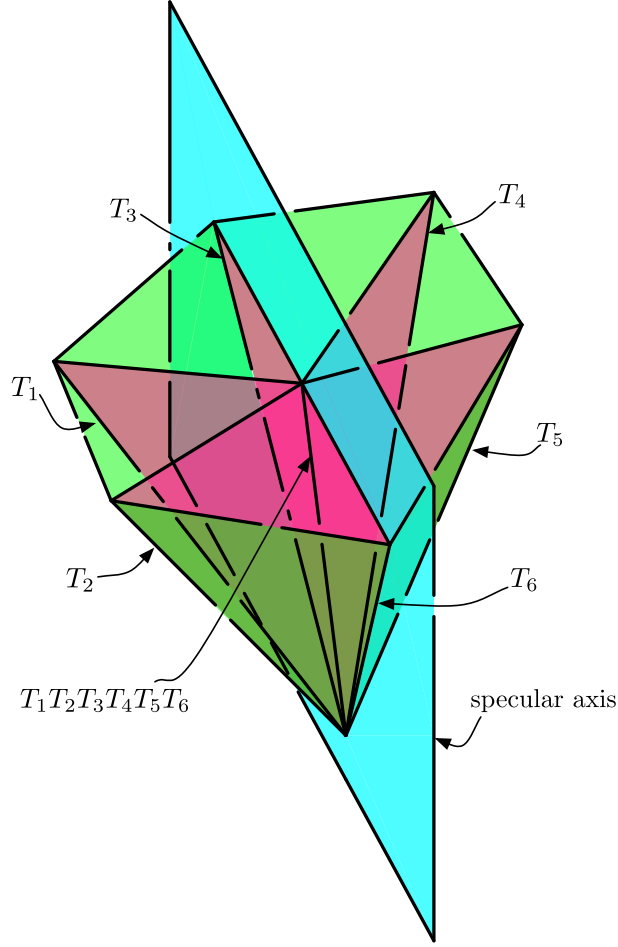


Figure 13. *The Specular Axis.* This is a schematic illustration of the master space cone of Models 13 and 15b. The rays corresponding to the basis of the cone are labelled with the associated fugacities T_i of the Hilbert series. The cone is symmetric along a hyperplane which we call the specular axis.

Model 13, the fugacity map

$$T_1 = x, T_2 = \tilde{f}, T_3 = b, T_4 = h_1, T_5 = h_2, T_6 = \frac{\tilde{t}}{x\tilde{f}bh_1h_2}, \quad (4.22)$$

rewrites the Hilbert series and plethystic logarithm such that they are related to the ones from Model 15b via

$$(T_1, T_2, T_3, T_4, T_5, T_6) \leftrightarrow (T_4, T_5, T_3, T_1, T_2, T_6) . \quad (4.23)$$

Note that the above map for fugacities T_i relates to the one for global symmetry fugacities in (4.19).

Given that the fugacities T_i relate to the boundary of the Calabi-Yau cone, the above fugacity map can be interpreted as a reflection along a hyperplane which is associated to monomials of the form $T_3^{m_3}T_6^{m_6}$. We call the hyperplane the **specular axis**. It is schematically illustrated in Figure 13.

The generators of the master space in terms of perfect matchings of Model 13 and Model 15b are shown with the corresponding global symmetry charges in Table 4 and Table 5 respectively. The master space cone with a selection of generators and the specular axis are illustrated schematically in Figure 14. Specular duality maps generators into each other along the specular axis.

generator	fields	$SU(2)_x$	$U(1)_f$	$SU(2)_{h_1}$	$SU(2)_{h_2}$	$U(1)_b$	$U(1)_R$	fugacity
$p_3 s_1 s_3$	X_{24}	0	-2	+1	+1	0	1/3	$T_1^2 T_3^2 T_4^3 T_5^3 T_6^2$
$p_3 s_1 s_4$	X_{41}^1	0	-2	+1	-1	0	1/3	$T_1^2 T_3^2 T_4^3 T_5 T_6^2$
$p_3 s_2 s_3$	X_{41}^1	0	-2	-1	+1	0	1/3	$T_1^2 T_3^2 T_4 T_5^3 T_6^2$
$p_3 s_2 s_4$	X_{42}	0	-2	-1	-1	0	1/3	$T_1^2 T_3^2 T_4 T_5 T_6^2$
$p_1 q_1 s_1$	X_{13}	+1	+1	+1	0	+1	1/3	$T_1^2 T_2^2 T_3^2 T_4^2 T_5 T_6$
$p_1 q_1 s_2$	X_{12}^2	+1	+1	-1	0	+1	1/3	$T_1^2 T_2^2 T_3^2 T_5 T_6$
$p_2 q_1 s_1$	X_{34}^2	-1	+1	+1	0	+1	1/3	$T_2^2 T_3^2 T_4^2 T_5 T_6$
$p_2 q_1 s_2$	X_{34}^1	-1	+1	-1	0	+1	1/3	$T_2^2 T_3^2 T_5 T_6$
$p_1 q_2 s_3$	X_{12}^1	+1	+1	0	+1	-1	1/3	$T_1^2 T_2^2 T_4 T_5^2 T_6$
$p_1 q_2 s_4$	X_{31}	+1	+1	0	-1	-1	1/3	$T_1^2 T_2^2 T_4 T_6$
$p_2 q_2 s_3$	X_{23}^2	-1	+1	0	+1	-1	1/3	$T_2^2 T_4 T_5^2 T_6$
$p_2 q_2 s_4$	X_{23}^1	-1	+1	0	-1	-1	1/3	$T_2^2 T_4 T_6$

Table 4. The generators of the master space of Model 13 with the corresponding charges under the global symmetry.

generator	fields	$SU(2)_x$	$SU(2)_y$	$SU(2)_{h_1}$	$U(1)_{h_2}$	$U(1)_b$	$U(1)_R$	fugacity
$p_1 p_3 s_3$	X_{42}^2	+1	+1	0	-2	0	1	$T_1^3 T_2^3 T_3^2 T_4^2 T_6^2$
$p_1 p_4 s_3$	X_{42}^4	+1	-1	0	-2	0	1	$T_1^3 T_2 T_3^2 T_4^2 T_6^2$
$p_2 p_3 s_3$	X_{42}^3	-1	+1	0	-2	0	1	$T_1 T_2^3 T_3^2 T_4^2 T_6^2$
$p_2 p_4 s_3$	X_{42}^1	-1	-1	0	-2	0	1	$T_1 T_2 T_3^2 T_4^2 T_6^2$
$p_1 s_1 s_4$	X_{21}^1	+1	0	+1	+1	+1	1/2	$T_1^2 T_2 T_3^2 T_4^2 T_5^2 T_6$
$p_2 s_1 s_4$	X_{21}^2	-1	0	+1	+1	+1	1/2	$T_2 T_3^2 T_4^2 T_5^2 T_6$
$p_1 s_2 s_4$	X_{34}^2	+1	0	-1	+1	+1	1/2	$T_1^2 T_2 T_3^2 T_5^2 T_6$
$p_2 s_2 s_4$	X_{34}^1	-1	0	-1	+1	+1	1/2	$T_2 T_3^2 T_5^2 T_6$
$p_3 s_1 s_5$	X_{23}^2	0	+1	+1	+1	-1	1/2	$T_1 T_2^2 T_4^2 T_5^2 T_6$
$p_4 s_1 s_5$	X_{23}^1	0	-1	+1	+1	-1	1/2	$T_1 T_4^2 T_5^2 T_6$
$p_3 s_2 s_5$	X_{14}^1	0	+1	-1	+1	-1	1/2	$T_1 T_2^2 T_5^2 T_6$
$p_4 s_2 s_5$	X_{14}^2	0	-1	-1	+1	-1	1/2	$T_1 T_5^2 T_6$

Table 5. The generators of the master space of Model 15b with the corresponding charges under the global symmetry.

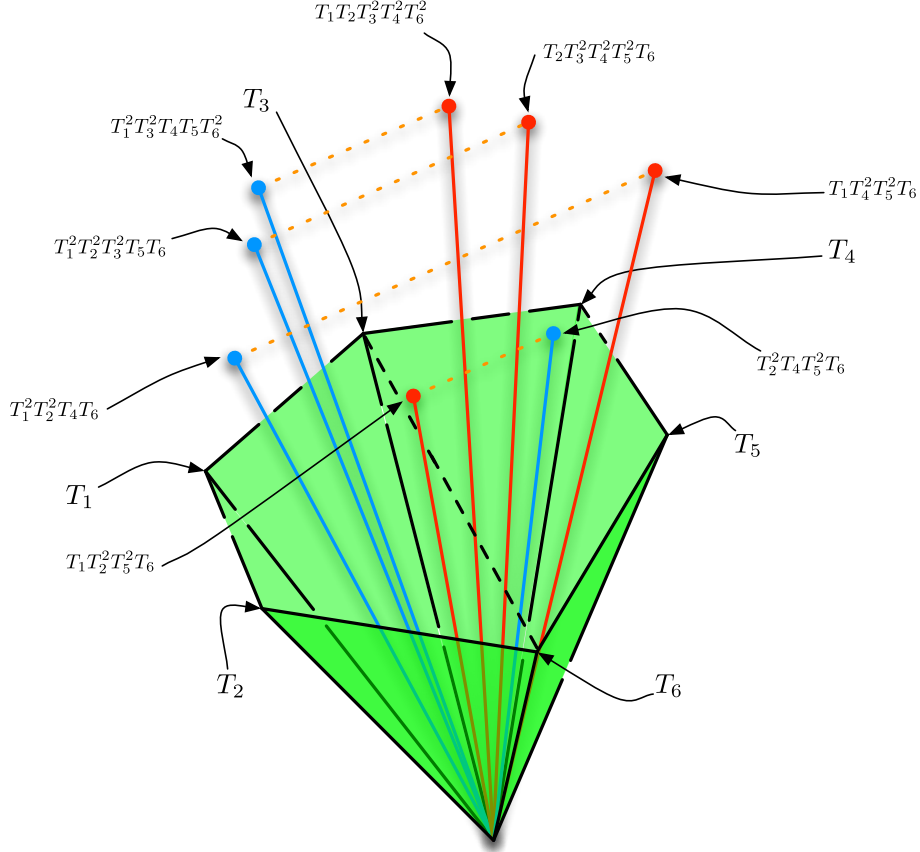


Figure 14. *The Specular Axis and Moduli Space Generators.* The schematic illustration shows a selection of master space generators of Model 15b and Model 13 which are highlighted in red and blue respectively. The dotted lines indicate the identifications of generators under specular duality.

5 Beyond the torus and Conclusions

Our work discusses specular duality between brane tilings which represent $4d \mathcal{N} = 1$ supersymmetric gauge theories with toric Calabi-Yau moduli spaces.

Starting from the observations made in [17], this paper identifies the following properties of specular duality for brane tilings on \mathbb{T}^2 with reflexive toric diagrams:

- Dual brane tilings have the same master space $^{\text{Irr}}\mathcal{F}^b$. The corresponding Hilbert series are the same up to a fugacity map.
- The new correspondence swaps internal and external perfect matchings.
- Mesonic flavor and anomalous or hidden baryonic symmetries are interchanged.

- Specular duality represents a hyperplane along which the cone of ${}^{\text{Irr}}\mathcal{F}^{\flat}$ is symmetric.

The new duality is an automorphism of the set of 30 brane tilings with reflexive toric diagrams [17].

When specular duality acts on a brane tiling whose toric diagram is not reflexive, the dual brane tiling is either on a sphere or on a Riemann surface of genus 2 or higher. Such brane tilings have no known AdS duals and their mesonic moduli spaces are not necessarily Calabi-Yau 3-folds [23, 31, 32].

In general, the number of faces G of a brane tiling relates to the number of faces \tilde{G} of the dual tiling by

$$\tilde{G} = E = G - 2I + 2 . \quad (5.1)$$

I and E are respectively the number of internal and external toric points for the original brane tiling.

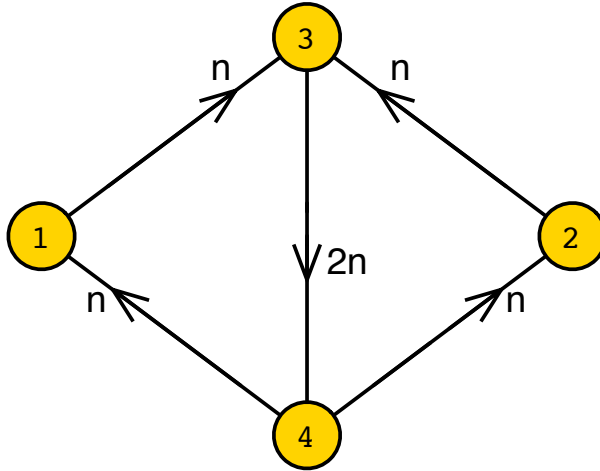


Figure 15. The quiver of the specular dual of the brane tiling for the Abelian orbifold of the form $\mathbb{C}^3/\mathbb{Z}_{2n}$ with orbifold action $(1, 1, -2)$ [33].

First examples of brane tilings on Riemann surfaces can be generated from Abelian orbifolds of \mathbb{C}^3 [53–57]. Consider the brane tilings which correspond to the Abelian orbifolds of the form $\mathbb{C}^3/\mathbb{Z}_{2n}$ with orbifold action $(1, 1, -2)$ and $n > 0$. The dual brane tiling is on a Riemann surface of genus $n - 1$. For the first few examples with $n = 1, 2, 3$,

the superpotentials are

$$W_{\mathbb{C}^3/\widetilde{\mathbb{Z}}_{2,(1,1,0)}} = X_{34}^1 X_{41} X_{13} + X_{34}^2 X_{42} X_{23} - X_{34}^2 X_{41} X_{13} - X_{34}^1 X_{42} X_{23} \quad , \quad (5.2)$$

$$W_{\mathbb{C}^3/\widetilde{\mathbb{Z}}_{4,(1,1,2)}} = X_{34}^1 X_{41}^1 X_{13}^1 + X_{34}^2 X_{42}^1 X_{23}^1 + X_{34}^3 X_{41}^2 X_{13}^2 + X_{34}^4 X_{42}^2 X_{23}^2 \\ - X_{34}^4 X_{41}^2 X_{13}^1 - X_{34}^1 X_{42}^2 X_{23}^1 - X_{34}^2 X_{41}^1 X_{13}^2 - X_{34}^3 X_{42}^1 X_{23}^2 \quad , \quad (5.3)$$

$$W_{\mathbb{C}^3/\widetilde{\mathbb{Z}}_{6,(1,1,4)}} = X_{34}^1 X_{41}^1 X_{13}^1 + X_{34}^2 X_{42}^1 X_{23}^1 + X_{34}^3 X_{41}^2 X_{13}^2 + X_{34}^4 X_{42}^2 X_{23}^2 \\ + X_{34}^5 X_{41}^3 X_{13}^3 + X_{34}^6 X_{42}^3 X_{23}^3 - X_{34}^6 X_{41}^3 X_{13}^1 - X_{34}^1 X_{42}^3 X_{23}^1 \\ - X_{34}^2 X_{41}^1 X_{13}^2 - X_{34}^3 X_{42}^1 X_{23}^2 - X_{34}^4 X_{41}^2 X_{13}^3 - X_{34}^5 X_{42}^2 X_{23}^3 \quad . \quad (5.4)$$

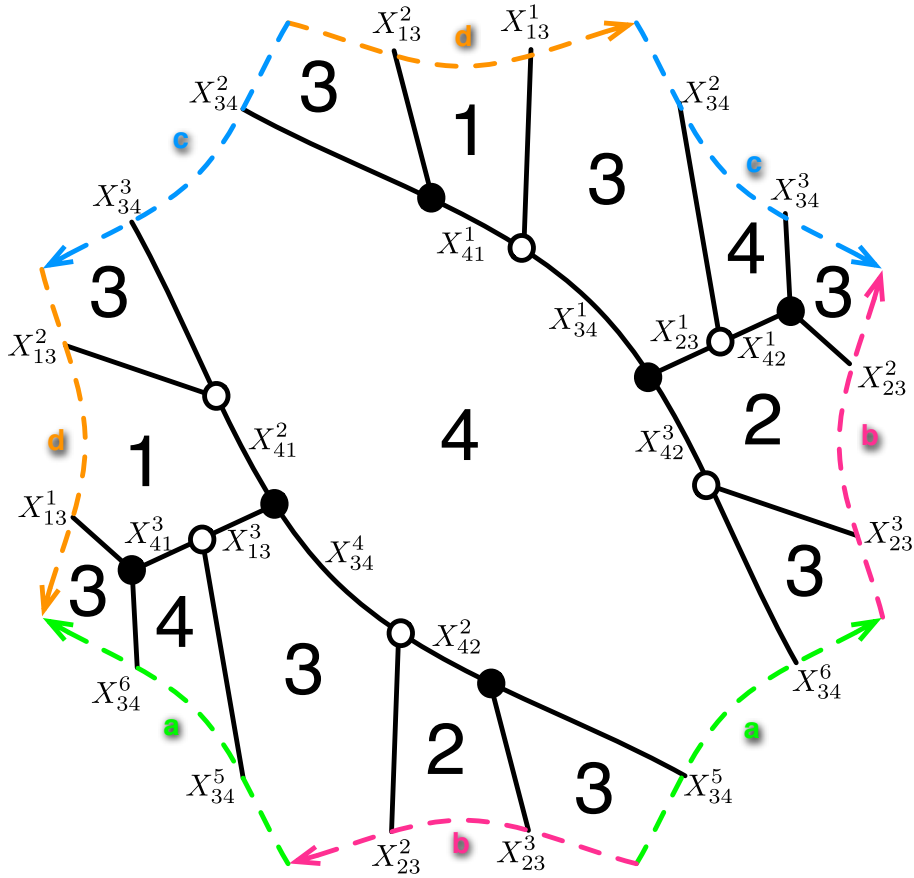


Figure 16. *Brane Tiling on a $g = 2$ Riemann Surface.* The figure shows the octagonal fundamental domain of the brane tiling which is the specular dual of $\mathbb{C}^3/\mathbb{Z}_6$ with action $(1, 1, 4)$.

The corresponding quivers are shown in Figure 15. The Hilbert series of the master

spaces are,

$$\begin{aligned}
g_1(t; \widetilde{\mathbb{C}^3/\mathbb{Z}_{2,(1,1,0)}}) &= \frac{1-t^4}{(1-t)(1-t^2)^4} \quad , \\
g_1(t; \widetilde{\mathbb{C}^3/\mathbb{Z}_{4,(1,1,2)}}) &= \frac{1+6t^3+6t^6+t^9}{(1-t^3)^6} \quad , \\
g_1(t; \widetilde{\mathbb{C}^3/\mathbb{Z}_{6,(1,1,4)}}) &= (1+3t^2+7t^4+18t^6+38t^8+72t^{10}+122t^{12}+186t^{14}+267t^{16} \\
&\quad +363t^{18}+456t^{20}+537t^{22}+588t^{24}+603t^{26}+588t^{28}+537t^{30}+456t^{32} \\
&\quad +363t^{34}+267t^{36}+186t^{38}+122t^{40}+72t^{42}+38t^{44}+18t^{46}+7t^{48} \\
&\quad +3t^{50}+t^{52}) \times \frac{(1-t^2)^3(1-t^4)}{(1-t^6)^7(1-t^8)^5} \quad . \tag{5.5}
\end{aligned}$$

The fundamental domain of the brane tiling for the specular dual of $\mathbb{C}^3/\mathbb{Z}_{6,(1,1,4)}$ is in Figure 16. It is of great interest to study such brane tilings on higher genus Riemann surfaces. One obtains a new class of quivers and field theories via specular duality which is the subject of a future investigation [33].

Acknowledgements

We like to thank S. Cremonesi, S. Franco and G. Torri for fruitful discussions. We also thank J. Stienstra for interesting correspondence. A. H. thanks Stanford University and SLAC for the kind hospitality during various stages of this project. R.-K. S. is grateful to the Simons Center for Geometry and Physics at Stony Brook University and the Hebrew University of Jerusalem for kind hospitality.

A Comments on mesonic and baryonic symmetry charges

Mesonic Symmetry. The mesonic moduli space of a given brane tiling on \mathbb{T}^2 is a non-compact toric Calabi-Yau 3-fold. The mesonic symmetry of the quiver gauge theory has rank 3 and hence takes one of the following forms,

- $U(1) \times U(1) \times U(1)$
- $SU(2) \times U(1) \times U(1)$
- $SU(2) \times SU(2) \times U(1)$
- $SU(3) \times U(1)$,

where the R-symmetry is a subgroup. For $\mathcal{N} = 2$ and $\mathcal{N} = 1$, the R-symmetry is respectively $SU(2) \times U(1)$ and $U(1)$.

The above global symmetries derive from the isometry group of the Calabi-Yau 3-fold. The enhancement of a $U(1)$ flavor to $SU(2)$ or $SU(3)$ is indicated by columns in the total charge matrix Q_t which carry the same charge and correspond to external perfect matchings.

Baryonic Symmetry. The baryonic symmetry is $U(1)^{G-1}$ or an enhancement with rank $G - 1$. It is divided into an anomalous and non-anomalous part. The anomalous $U(1)$ baryonic symmetries can appear as enhanced non-Abelian symmetries which are known as hidden symmetries. These are isometries of the master space, but are not a symmetry of the Lagrangian. They are indicated by non-extremal perfect matchings which carry the same Q_F charge. The number of anomalous $U(1)$ baryonic symmetries or the rank of the hidden symmetry is given by twice the number of internal points in the associated toric diagram, $2I$. The non-anomalous baryonic $U(1)$ symmetries are given by $E - 3$ where E is the number of external toric points.

Mesonic and Baryonic Charges on perfect matchings. The perfect matchings carry $G + 2$ charges which relate to the 3 mesonic and $G - 1$ baryonic symmetries. Each perfect matching is assigned a $G + 2$ dimensional charge vector, and the choice of its components is arbitrary up to the following constraints:

- All $G + 2$ dimensional charge vectors are linearly independent to each other.
- The sum of all charge vectors is $(0, \dots, 0, 2)$ where the non-zero component 2 is the total $U(1)_R$ -charge.

Note that if two charge vectors are linearly dependent, information about the algebraic structure of the moduli space is lost. For the purpose of studying specular duality, the following additional constraints are introduced without losing track of the algebraic structure of the master space:

- For a pair of dual brane tilings, the charge vectors can be chosen such that a swap between internal and external perfect matchings equates to a swap of mesonic flavour and anomalous or hidden baryonic symmetry charges.
- If the $U(1)_R$ -charges are irrational or otherwise incompatible between dual brane tilings, one can find a set of orthogonal replacement charges without losing information on the algebraic structure of the master space. This modification corresponds to a mix of the R-symmetry with the remaining global symmetry.

B Hilbert series of $\text{Irr } \mathcal{F}^\flat$ for Models 13 and 15b

The refined Hilbert series of the master space of Model 15b, and by specular duality of the master space of Model 13, is of the form

$$g_1(t_i, y_{s_i}; \text{Irr } \mathcal{F}_{15b}^\flat) = \frac{P(t_i, y_{s_i})}{(1 - t_1 t_2 y_{s_3})(1 - t_2 t_3 y_{s_3})(1 - t_1 t_4 y_{s_3})(1 - t_2 t_4 y_{s_3})} \times \frac{1}{(1 - t_1 s_1 y_{s_4})(1 - t_2 s_1 y_{s_4})(1 - t_1 y_{s_2} y_{s_4})(1 - t_2 y_{s_2} y_{s_4})} \times \frac{1}{(1 - t_3 y_{s_1} y_{s_5})(1 - t_4 y_{s_1} y_{s_5})(1 - t_3 y_{s_2} y_{s_5})(1 - t_4 y_{s_2} y_{s_5})} , \quad (\text{B.1})$$

where the numerator is

$$\begin{aligned} P(t_i, s_i) = & 1 - t_1 t_2 t_3 t_4 y_{s_3}^2 - t_1 t_2 t_3 y_{s_1} y_{s_3} y_{s_4} - t_1 t_2 t_4 y_{s_1} y_{s_3} y_{s_4} - t_1 t_2 t_3 y_{s_2} y_{s_3} y_{s_4} - t_1 t_2 t_4 y_{s_2} y_{s_3} y_{s_4} \\ & + t_1^2 t_2 t_3 t_4 y_{s_1} y_{s_3} y_{s_4}^2 + t_1 t_2^2 t_3 t_4 y_{s_1} y_{s_3} y_{s_4}^2 + t_1^2 t_2 t_3 t_4 y_{s_2} y_{s_3} y_{s_4}^2 + t_1 t_2^2 t_3 t_4 y_{s_2} y_{s_3} y_{s_4}^2 - t_1 t_2 y_{s_1} y_{s_2} y_{s_4}^2 \\ & + t_1^2 t_2 t_3 y_{s_1} y_{s_2} y_{s_3} y_{s_4}^2 + t_1 t_2^2 t_3 y_{s_1} y_{s_2} y_{s_3} y_{s_4}^2 + t_1^2 t_2 t_4 y_{s_1} y_{s_2} y_{s_3} y_{s_4}^2 + t_1 t_2^2 t_4 y_{s_1} y_{s_2} y_{s_3} y_{s_4}^2 - t_1^3 t_2 t_3 t_4 y_{s_1} y_{s_2} y_{s_3} y_{s_4}^2 \\ & - t_1^2 t_2^2 t_3 t_4 y_{s_1} y_{s_2} y_{s_3} y_{s_4}^2 - t_1 t_2^3 t_3 t_4 y_{s_1} y_{s_2} y_{s_3} y_{s_4}^2 - t_1 t_3 t_4 y_{s_1} y_{s_3} y_{s_5} - t_2 t_3 t_4 y_{s_1} y_{s_3} y_{s_5} - t_1 t_3 t_4 y_{s_2} y_{s_3} y_{s_5} \\ & - t_2 t_3 t_4 y_{s_2} y_{s_3} y_{s_5} + t_1 t_2 t_3^2 t_4 y_{s_1} y_{s_3} y_{s_5}^2 + t_1 t_2 t_3 t_4^2 y_{s_1} y_{s_3} y_{s_5}^2 + t_1 t_2 t_3 t_4 y_{s_2} y_{s_3} y_{s_5}^2 + t_1 t_2 t_3 t_4^2 y_{s_2} y_{s_3} y_{s_5}^2 \\ & - t_1 t_3 y_{s_1} y_{s_2} y_{s_4} y_{s_5} - t_2 t_3 y_{s_1} y_{s_2} y_{s_4} y_{s_5} - t_1 t_4 y_{s_1} y_{s_2} y_{s_4} y_{s_5} - t_2 t_4 y_{s_1} y_{s_2} y_{s_4} y_{s_5} + t_1 t_2 t_3 t_4 y_{s_1}^2 y_{s_3} y_{s_4} y_{s_5} \\ & + t_1 t_2 t_3^2 y_{s_1} y_{s_2} y_{s_3} y_{s_4} y_{s_5} + t_1^2 t_3 t_4 y_{s_1} y_{s_2} y_{s_3} y_{s_4} y_{s_5} + 5 t_1 t_2 t_3 t_4 y_{s_1} y_{s_2} y_{s_3} y_{s_4} y_{s_5} + t_2^2 t_3 t_4 y_{s_1} y_{s_2} y_{s_3} y_{s_4} y_{s_5} \\ & + t_1 t_2 t_4^2 y_{s_1} y_{s_2} y_{s_3} y_{s_4} y_{s_5} + t_1 t_2 t_3 t_4 y_{s_2}^2 y_{s_3} y_{s_4} y_{s_5} - t_1^2 t_2^2 t_3^2 t_4 y_{s_1} y_{s_2} y_{s_3}^2 y_{s_4} y_{s_5} - t_1 t_2^2 t_3^2 t_4 y_{s_1} y_{s_2} y_{s_3}^2 y_{s_4} y_{s_5} \\ & - t_1^2 t_2 t_3 t_4^2 y_{s_1} y_{s_2} y_{s_3}^2 y_{s_4} y_{s_5} - t_1 t_2^2 t_3 t_4^2 y_{s_1} y_{s_2} y_{s_3}^2 y_{s_4} y_{s_5} - t_1^2 t_2^2 t_3^2 t_4^2 y_{s_1} y_{s_2} y_{s_3}^3 y_{s_4} y_{s_5} - t_1 t_2^2 t_3^2 t_4^2 y_{s_1} y_{s_2} y_{s_3}^3 y_{s_4} y_{s_5} \\ & - t_1^2 t_2^2 t_3^2 t_4^2 y_{s_1}^2 y_{s_2} y_{s_3}^3 y_{s_4} y_{s_5} + t_1 t_2 t_3 y_{s_1}^2 y_{s_2} y_{s_4}^2 y_{s_5} + t_1 t_2 t_3 y_{s_1} y_{s_2}^2 y_{s_4}^2 y_{s_5} \\ & + t_1 t_2 t_4 y_{s_1} y_{s_2}^2 y_{s_4}^2 y_{s_5} - t_1^2 t_2 t_3 t_4 y_{s_1}^2 y_{s_2} y_{s_3} y_{s_4}^2 y_{s_5} - t_1 t_2^2 t_3 t_4 y_{s_1}^2 y_{s_2} y_{s_3} y_{s_4}^2 y_{s_5} - t_1^2 t_2^2 t_3^2 t_4 y_{s_1} y_{s_2}^2 y_{s_3}^2 y_{s_4}^2 y_{s_5} \\ & - t_1^2 t_2^2 t_3^2 t_4 y_{s_1} y_{s_2}^2 y_{s_3}^2 y_{s_4}^2 y_{s_5} + t_1^3 t_2^2 t_3^2 t_4 y_{s_1}^2 y_{s_2} y_{s_3}^3 y_{s_4}^2 y_{s_5} + t_1^2 t_2^3 t_3^2 t_4 y_{s_1}^2 y_{s_2} y_{s_3}^3 y_{s_4}^2 y_{s_5} \\ & + t_1^2 t_2^3 t_3^2 t_4 y_{s_1} y_{s_2}^2 y_{s_3}^3 y_{s_4}^2 y_{s_5} - t_1^2 t_2^2 t_3^2 y_{s_1}^2 y_{s_2} y_{s_3}^3 y_{s_4}^2 y_{s_5} - t_1^2 t_2^2 t_3^2 t_4 y_{s_1}^2 y_{s_2} y_{s_3}^3 y_{s_4}^2 y_{s_5} \\ & + t_1^3 t_2^2 t_3^2 t_4 y_{s_1}^2 y_{s_2} y_{s_3}^3 y_{s_4}^2 y_{s_5} + t_1^2 t_2^3 t_3^2 t_4 y_{s_1}^2 y_{s_2} y_{s_3}^3 y_{s_4}^2 y_{s_5} + t_1^2 t_2^3 t_3^2 t_4 y_{s_1}^2 y_{s_2} y_{s_3}^3 y_{s_4}^2 y_{s_5} \\ & - t_1^3 t_2^3 t_3^2 t_4 y_{s_1}^2 y_{s_2} y_{s_3}^3 y_{s_4}^2 y_{s_5} - t_3 t_4 y_{s_1} y_{s_2} y_{s_5}^2 + t_1 t_3^2 t_4 y_{s_1} y_{s_2} y_{s_3} y_{s_5}^2 + t_2 t_3^2 t_4 y_{s_1} y_{s_2} y_{s_3} y_{s_5}^2 \\ & + t_1 t_3 t_4^2 y_{s_1} y_{s_2} y_{s_3} y_{s_5}^2 + t_2 t_3 t_4^2 y_{s_1} y_{s_2} y_{s_3} y_{s_5}^2 - t_1 t_2 t_3^2 t_4 y_{s_1} y_{s_2} y_{s_3}^2 y_{s_5}^2 - t_1 t_2 t_3^2 t_4 y_{s_1} y_{s_2} y_{s_3}^2 y_{s_5}^2 \\ & - t_1 t_2 t_3 t_4^3 y_{s_1} y_{s_2} y_{s_3} y_{s_5}^2 + t_1 t_3 t_4 y_{s_1}^2 y_{s_2} y_{s_4} y_{s_5}^2 + t_2 t_3 t_4 y_{s_1}^2 y_{s_2} y_{s_4} y_{s_5}^2 + t_1 t_3 t_4 y_{s_1} y_{s_2}^2 y_{s_4} y_{s_5}^2 \\ & + t_2 t_3 t_4 y_{s_1} y_{s_2}^2 y_{s_4} y_{s_5}^2 - t_1 t_2 t_3^2 t_4 y_{s_1}^2 y_{s_2} y_{s_3} y_{s_4} y_{s_5}^2 - t_1 t_2 t_3 t_4^2 y_{s_1}^2 y_{s_2} y_{s_3} y_{s_4} y_{s_5}^2 - t_1 t_2 t_3^2 t_4 y_{s_1} y_{s_2}^2 y_{s_3} y_{s_4} y_{s_5}^2 \\ & - t_1 t_2 t_3 t_4^2 y_{s_1} y_{s_2}^2 y_{s_3} y_{s_4} y_{s_5}^2 - t_1^2 t_2^2 t_3^2 t_4^2 y_{s_1}^2 y_{s_2} y_{s_3}^2 y_{s_4} y_{s_5}^2 - t_1 t_2^2 t_3^2 t_4^2 y_{s_1} y_{s_2} y_{s_3}^2 y_{s_4} y_{s_5}^2 - t_1^2 t_2^2 t_3^2 t_4^2 y_{s_1} y_{s_2}^2 y_{s_3}^2 y_{s_4} y_{s_5}^2 \end{aligned}$$

$$\begin{aligned}
& -t_1 t_2^2 t_3^2 t_4^2 y_{s_1} y_{s_2}^2 y_{s_3}^2 y_{s_4} y_{s_5}^2 + t_1^2 t_2^2 t_3^2 t_4^2 y_{s_1}^2 y_{s_2} y_{s_3}^3 y_{s_4} y_{s_5}^2 + t_1^2 t_2^2 t_3^2 t_4^3 y_{s_1}^2 y_{s_2} y_{s_3}^3 y_{s_4} y_{s_5}^2 + t_1^2 t_2^2 t_3^2 t_4^2 y_{s_1} y_{s_2}^2 y_{s_3}^3 y_{s_4} y_{s_5}^2 \\
& + t_1^2 t_2^2 t_3^2 t_4^3 y_{s_1} y_{s_2}^2 y_{s_3}^3 y_{s_4} y_{s_5}^2 - t_1 t_2 t_3 t_4 y_{s_1}^3 y_{s_2} y_{s_4} y_{s_5}^2 - t_1 t_2 t_3 t_4 y_{s_1}^2 y_{s_2}^2 y_{s_4} y_{s_5}^2 - t_1 t_2 t_3 t_4 y_{s_1} y_{s_2}^3 y_{s_4} y_{s_5}^2 \\
& - t_1^2 t_2^2 t_3^2 t_4^2 y_{s_1}^2 y_{s_2}^2 y_{s_3} y_{s_4}^2 y_{s_5}^2 - t_1 t_2^2 t_3^2 t_4^2 y_{s_1}^2 y_{s_2}^2 y_{s_3} y_{s_4}^2 y_{s_5}^2 - t_1^2 t_2^2 t_3^2 t_4^2 y_{s_1}^2 y_{s_2}^2 y_{s_3} y_{s_4}^2 y_{s_5}^2 - t_1 t_2^2 t_3^2 t_4^2 y_{s_1}^2 y_{s_2}^2 y_{s_3} y_{s_4}^2 y_{s_5}^2 \\
& + t_1^2 t_2^2 t_3^2 t_4^2 y_{s_1}^3 y_{s_2} y_{s_3}^2 y_{s_4}^2 y_{s_5}^2 + t_1^2 t_2^2 t_3^2 t_4^2 y_{s_1}^2 y_{s_2}^2 y_{s_3}^2 y_{s_4}^2 y_{s_5}^2 + t_1^3 t_2^2 t_3^2 t_4^2 y_{s_1}^2 y_{s_2}^2 y_{s_3}^2 y_{s_4}^2 y_{s_5}^2 + 5 t_1^2 t_2^2 t_3^2 t_4^2 y_{s_1}^2 y_{s_2}^2 y_{s_3}^2 y_{s_4}^2 y_{s_5}^2 \\
& + t_1 t_2^3 t_3^2 t_4^2 y_{s_1}^2 y_{s_2}^2 y_{s_3}^2 y_{s_4}^2 y_{s_5}^2 + t_1^2 t_2^2 t_3^3 t_4^2 y_{s_1}^2 y_{s_2}^2 y_{s_3}^2 y_{s_4}^2 y_{s_5}^2 + t_1^2 t_2^2 t_3^2 t_4^2 y_{s_1} y_{s_2}^3 y_{s_3}^2 y_{s_4}^2 y_{s_5}^2 - t_1^3 t_2^2 t_3^2 t_4^2 y_{s_1}^2 y_{s_2}^2 y_{s_3}^3 y_{s_4}^2 y_{s_5}^2 \\
& - t_1^2 t_2^3 t_3^2 t_4^2 y_{s_1}^2 y_{s_2}^2 y_{s_3}^3 y_{s_4}^2 y_{s_5}^2 - t_1^3 t_2^2 t_3^2 t_4^2 y_{s_1}^2 y_{s_2}^2 y_{s_3}^3 y_{s_4}^2 y_{s_5}^2 - t_1^2 t_2^3 t_3^2 t_4^2 y_{s_1}^2 y_{s_2}^2 y_{s_3}^3 y_{s_4}^2 y_{s_5}^2 + t_1^2 t_2^2 t_3^2 t_4^2 y_{s_1}^3 y_{s_2}^2 y_{s_3}^3 y_{s_4}^2 y_{s_5}^2 \\
& + t_1^2 t_2^2 t_3^2 t_4^2 y_{s_1}^2 y_{s_2}^3 y_{s_3}^3 y_{s_4}^2 y_{s_5}^2 + t_1^2 t_2^2 t_3^2 t_4^2 y_{s_1}^2 y_{s_2}^3 y_{s_3}^3 y_{s_4}^2 y_{s_5}^2 + t_1^2 t_2^2 t_3^2 t_4^2 y_{s_1}^2 y_{s_2}^3 y_{s_3}^3 y_{s_4}^2 y_{s_5}^2 - t_1^3 t_2^2 t_3^2 t_4^2 y_{s_1}^2 y_{s_2}^2 y_{s_3}^3 y_{s_4}^2 y_{s_5}^2 \\
& - t_1^2 t_2^3 t_3^2 t_4^2 y_{s_1}^3 y_{s_2}^2 y_{s_3}^3 y_{s_4}^2 y_{s_5}^2 - t_1^3 t_2^2 t_3^2 t_4^2 y_{s_1}^2 y_{s_2}^3 y_{s_3}^3 y_{s_4}^2 y_{s_5}^2 - t_1^2 t_2^3 t_3^2 t_4^2 y_{s_1}^2 y_{s_2}^3 y_{s_3}^3 y_{s_4}^2 y_{s_5}^2 - t_1^2 t_2^3 t_3^2 t_4^2 y_{s_1}^2 y_{s_2}^3 y_{s_3}^3 y_{s_4}^2 y_{s_5}^2 \\
& - t_1 t_2 t_3^2 t_4^2 y_{s_1}^2 y_{s_2}^2 y_{s_3} y_{s_4} y_{s_5}^3 - t_2^2 t_3^2 t_4^2 y_{s_1}^2 y_{s_2}^2 y_{s_3} y_{s_4} y_{s_5}^3 + t_1^2 t_2 t_3^2 t_4^2 y_{s_1}^2 y_{s_2}^2 y_{s_3} y_{s_4} y_{s_5}^3 + t_1 t_2^2 t_3^2 t_4^2 y_{s_1}^2 y_{s_2}^2 y_{s_3}^2 y_{s_4} y_{s_5}^3 \\
& + t_1^2 t_2 t_3^2 t_4^3 y_{s_1}^2 y_{s_2}^2 y_{s_3}^2 y_{s_4} y_{s_5}^3 + t_1 t_2^2 t_3^2 t_4^3 y_{s_1}^2 y_{s_2}^2 y_{s_3}^2 y_{s_4} y_{s_5}^3 - t_1^2 t_2^2 t_3^2 t_4^3 y_{s_1}^2 y_{s_2}^2 y_{s_3}^3 y_{s_4} y_{s_5}^3 + t_1^2 t_2^2 t_3^2 t_4^2 y_{s_1}^3 y_{s_2}^2 y_{s_3}^2 y_{s_4} y_{s_5}^3 \\
& + t_1 t_2^2 t_3^2 t_4^2 y_{s_1}^2 y_{s_2}^3 y_{s_3}^2 y_{s_4} y_{s_5}^3 + t_1^2 t_2^2 t_3^2 t_4^2 y_{s_1}^2 y_{s_2}^3 y_{s_3}^2 y_{s_4} y_{s_5}^3 + t_1 t_2^2 t_3^2 t_4^2 y_{s_1}^2 y_{s_2}^3 y_{s_3}^2 y_{s_4} y_{s_5}^3 - t_1^2 t_2^2 t_3^2 t_4^2 y_{s_1}^2 y_{s_2}^2 y_{s_3}^2 y_{s_4}^2 y_{s_5}^3 \\
& - t_1^2 t_2^2 t_3^2 t_4^3 y_{s_1}^3 y_{s_2}^2 y_{s_3}^2 y_{s_4} y_{s_5}^3 - t_1^2 t_2^2 t_3^2 t_4^2 y_{s_1}^2 y_{s_2}^3 y_{s_3}^2 y_{s_4} y_{s_5}^3 - t_1^2 t_2^2 t_3^2 t_4^2 y_{s_1}^2 y_{s_2}^3 y_{s_3}^2 y_{s_4} y_{s_5}^3 - t_1^2 t_2^2 t_3^2 t_4^2 y_{s_1}^2 y_{s_2}^3 y_{s_3}^2 y_{s_4} y_{s_5}^3 \\
& + t_1^3 t_2^2 t_3^2 t_4^2 y_{s_1}^3 y_{s_2}^2 y_{s_3}^3 y_{s_4} y_{s_5}^3 . \tag{B.2}
\end{aligned}$$

References

- [1] W. Lerche, C. Vafa, and N. P. Warner, *Chiral Rings in N=2 Superconformal Theories*, *Nucl. Phys.* **B324** (1989) 427.
- [2] P. Candelas, M. Lynker, and R. Schimmrigk, *Calabi-Yau Manifolds in Weighted P(4)*, *Nucl. Phys.* **B341** (1990) 383–402.
- [3] B. R. Greene and M. R. Plesser, *Duality in Calabi-Yau Moduli Space*, *Nucl. Phys.* **B338** (1990) 15–37.
- [4] D. R. Morrison, *Mirror symmetry and rational curves on quintic threefolds: a guide for mathematicians*, *J.AMER.MATH.SOC.* **6** (1993) 223.
- [5] V. V. Batyrev, *Dual polyhedra and mirror symmetry for Calabi-Yau hypersurfaces in toric varieties*, *J. Alg. Geom.* **3** (1994) 493–545.
- [6] V. Batyrev and D. Dais, *Strong McKay correspondence, string theoretic Hodge numbers and mirror symmetry*, [alg-geom/9410001](#).
- [7] V. V. Batyrev and L. A. Borisov, *Dual cones and mirror symmetry for generalized Calabi-Yau manifolds*, . In *Greene, B. (ed.): Yau, S.T. (ed.): Mirror symmetry II* 71–86.

- [8] D. Cox and S. Katz, *Mirror symmetry and algebraic geometry*. Mathematical surveys and monographs. American Mathematical Society, 1999.
- [9] K. Hori, S. Katz, A. Klemm, R. Pandharipande, R. Thomas, C. Vafa, R. Vakil, and E. Zaslow, *Mirror symmetry*, vol. 1 of *Clay mathematics monographs*. American Mathematical Society, Providence, RI, 2003.
- [10] B. Feng, A. Hanany, and Y.-H. He, *D-brane gauge theories from toric singularities and toric duality*, *Nucl. Phys.* **B595** (2001) 165–200, [[hep-th/0003085](#)].
- [11] B. Feng, A. Hanany, and Y.-H. He, *Phase structure of D-brane gauge theories and toric duality*, *JHEP* **08** (2001) 040, [[hep-th/0104259](#)].
- [12] B. Feng, S. Franco, A. Hanany, and Y.-H. He, *Symmetries of toric duality*, *JHEP* **12** (2002) 076, [[hep-th/0205144](#)].
- [13] N. Seiberg, *Electric - magnetic duality in supersymmetric nonAbelian gauge theories*, *Nucl.Phys.* **B435** (1995) 129–146, [[hep-th/9411149](#)].
- [14] B. Feng, A. Hanany, Y.-H. He, and A. M. Uranga, *Toric duality as Seiberg duality and brane diamonds*, *JHEP* **12** (2001) 035, [[hep-th/0109063](#)].
- [15] C. E. Beasley and M. Ronen Plesser, *Toric duality is Seiberg duality*, *Journal of High Energy Physics* **12** (Dec., 2001) 1–+, [[hep-th/0109053](#)].
- [16] S. Franco, A. Hanany, and Y.-H. He, *A trio of dualities: Walls, trees and cascades*, *Fortsch. Phys.* **52** (2004) 540–547, [[hep-th/0312222](#)].
- [17] A. Hanany and R.-K. Seong, *Brane Tilings and Reflexive Polygons*, [arXiv:1201.2614](#).
- [18] A. Hanany and K. D. Kennaway, *Dimer models and toric diagrams*, [hep-th/0503149](#).
- [19] S. Franco, A. Hanany, K. D. Kennaway, D. Vegh, and B. Wecht, *Brane Dimers and Quiver Gauge Theories*, *JHEP* **01** (2006) 096, [[hep-th/0504110](#)].
- [20] S. Franco *et. al.*, *Gauge theories from toric geometry and brane tilings*, *JHEP* **01** (2006) 128, [[hep-th/0505211](#)].
- [21] A. Hanany and D. Vegh, *Quivers, tilings, branes and rhombi*, *JHEP* **10** (2007) 029, [[hep-th/0511063](#)].
- [22] A. Hanany, C. P. Herzog, and D. Vegh, *Brane tilings and exceptional collections*, *JHEP* **07** (2006) 001, [[hep-th/0602041](#)].
- [23] K. D. Kennaway, *Brane Tilings*, *Int. J. Mod. Phys.* **A22** (2007) 2977–3038, [[arXiv:0706.1660](#)].
- [24] M. Yamazaki, *Brane Tilings and Their Applications*, *Fortsch. Phys.* **56** (2008) 555–686, [[arXiv:0803.4474](#)].
- [25] M. Kreuzer and H. Skarke, *On the Classification of Reflexive Polyhedra*, *Communications in Mathematical Physics* **185** (1997) 495–508, [[hep-th/9512204](#)].

- [26] M. Kreuzer and H. Skarke, *Classification of Reflexive Polyhedra in Three Dimensions*, *Adv. Theor. Math. Phys.* **2** (1998) 847–864, [[hep-th/9805190](#)].
- [27] M. Kreuzer and H. Skarke, *Reflexive polyhedra, weights and toric Calabi-Yau fibrations*, *Rev. Math. Phys.* **14** (2002) 343–374, [[math/0001106](#)].
- [28] M. Kreuzer and H. Skarke, *Complete classification of reflexive polyhedra in four dimensions*, *Adv. Theor. Math. Phys.* **4** (2002) 1209–1230, [[hep-th/0002240](#)].
- [29] V. Batyrev and M. Kreuzer, *Constructing new Calabi-Yau 3-folds and their mirrors via conifold transitions*, *ArXiv e-prints* (Feb., 2008) [[arXiv:0802.3376](#)].
- [30] P. Candelas and R. Davies, *New Calabi-Yau Manifolds with Small Hodge Numbers*, *ArXiv e-prints* (Sept., 2008) [[arXiv:0809.4681](#)].
- [31] S. Benvenuti and A. Hanany, *New results on superconformal quivers*, *JHEP* **0604** (2006) 032, [[hep-th/0411262](#)].
- [32] S. Benvenuti and A. Hanany, *Conformal manifolds for the conifold and other toric field theories*, *JHEP* **0508** (2005) 024, [[hep-th/0502043](#)].
- [33] *work in progress*, .
- [34] B. Feng, Y.-H. He, K. D. Kennaway, and C. Vafa, *Dimer models from mirror symmetry and quivering amoebae*, *Adv.Theor.Math.Phys.* **12** (2008) 3, [[hep-th/0511287](#)].
- [35] S. Franco, *Dimer Models, Integrable Systems and Quantum Teichmuller Space*, *JHEP* **1109** (2011) 057, [[arXiv:1105.1777](#)].
- [36] J. Stienstra, *Hypergeometric Systems in two Variables, Quivers, Dimers and Dessins d’Enfants*, [arXiv:0711.0464](#).
- [37] A. Butti, D. Forcella, A. Hanany, D. Vegh, and A. Zaffaroni, *Counting Chiral Operators in Quiver Gauge Theories*, *JHEP* **11** (2007) 092, [[arXiv:0705.2771](#)].
- [38] S. Franco, A. Hanany, D. Krefl, J. Park, A. M. Uranga, *et. al.*, *Dimers and orientifolds*, *JHEP* **0709** (2007) 075, [[arXiv:0707.0298](#)].
- [39] A. Hanany, D. Vegh, and A. Zaffaroni, *Brane Tilings and M2 Branes*, *JHEP* **0903** (2009) 012, [[arXiv:0809.1440](#)].
- [40] D. Forcella, A. Hanany, Y.-H. He, and A. Zaffaroni, *The Master Space of N=1 Gauge Theories*, *JHEP* **0808** (2008) 012, [[arXiv:0801.1585](#)].
- [41] D. Forcella, A. Hanany, Y.-H. He, and A. Zaffaroni, *Mastering the Master Space*, *Lett.Math.Phys.* **85** (2008) 163–171, [[arXiv:0801.3477](#)].
- [42] A. Ishii and K. Ueda, *On moduli spaces of quiver representations associated with dimer models*, *ArXiv e-prints* (Oct., 2007) [[arXiv:0710.1898](#)].
- [43] E. Witten, *Phases of N = 2 theories in two dimensions*, *Nucl. Phys.* **B403** (1993) 159–222, [[hep-th/9301042](#)].

- [44] A. Hanany and A. Zaffaroni, *The master space of supersymmetric gauge theories*, *Adv.High Energy Phys.* **2010** (2010) 427891.
- [45] S. Benvenuti, B. Feng, A. Hanany, and Y.-H. He, *Counting BPS operators in gauge theories: Quivers, syzygies and plethystics*, *JHEP* **11** (2007) 050, [[hep-th/0608050](#)].
- [46] B. Feng, A. Hanany, and Y.-H. He, *Counting Gauge Invariants: the Plethystic Program*, *JHEP* **03** (2007) 090, [[hep-th/0701063](#)].
- [47] A. Hanany, *Counting BPS operators in the chiral ring: The plethystic story*, *AIP Conf.Proc.* **939** (2007) 165–175.
- [48] D. Forcella, A. Hanany, and A. Zaffaroni, *Master Space, Hilbert Series and Seiberg Duality*, *JHEP* **0907** (2009) 018, [[arXiv:0810.4519](#)].
- [49] K. Hori and C. Vafa, *Mirror symmetry*, [hep-th/0002222](#).
- [50] K. Hori, A. Iqbal, and C. Vafa, *D-branes and mirror symmetry*, [hep-th/0005247](#).
- [51] R. Kenyon and J.-M. Schlenker, *Rhombic embeddings of planar graphs with faces of degree 4*, *ArXiv Mathematical Physics e-prints* (May, 2003) [[math-ph/0](#)].
- [52] O. Aharony, A. Hanany, and B. Kol, *Webs of (p,q) 5-branes, five dimensional field theories and grid diagrams*, *JHEP* **01** (1998) 002, [[hep-th/9710116](#)].
- [53] A. Hanany, D. Orlando, and S. Reffert, *Sublattice Counting and Orbifolds*, *JHEP* **06** (2010) 051, [[arXiv:1002.2981](#)].
- [54] J. Davey, A. Hanany, and R.-K. Seong, *An Introduction to Counting Orbifolds*, *Fortsch. Phys.* **59** (2011) 677–682, [[arXiv:1102.0015](#)].
- [55] A. Hanany and R.-K. Seong, *Symmetries of Abelian Orbifolds*, *JHEP* **01** (2011) 027, [[arXiv:1009.3017](#)].
- [56] J. Davey, A. Hanany, and R.-K. Seong, *Counting Orbifolds*, *JHEP* **06** (2010) 010, [[arXiv:1002.3609](#)].
- [57] A. Hanany, V. Jejjala, S. Ramgoolam, and R.-K. Seong, *Calabi-Yau Orbifolds and Torus Coverings*, *JHEP* **09** (2011) 116, [[arXiv:1105.3471](#)].